Early nasal type I IFN immunity against SARS-CoV-2 is compromised in patients with autoantibodies against type I IFNs

Jonathan Lopez, Marine Mommert, William Mouton, Andrés Pizzorno, Karen Brengel-Pesce, Mehdi Mezidi, Marine Villard, Bruno Lina, Jean-Christophe Richard, Jean-Baptiste Fassier, et al.

JEM Journal of Experimental Medicine

ARTICLE

Early nasal type I IFN immunity against SARS-CoV-2 is compromised in patients with autoantibodies against type I IFNs

Jonathan Lopez[1*], Marine Mommert[2,3*], William Mouton[2,4*], Andrés Pizzorno[4*], Karen Brengel-Pesce[2*], Mehdi Mezidi[5], Marine Villard[4], Bruno Lina[4,6], Jean-Christophe Richard[5], Jean-Baptiste Fassier[7,8], Valérie Cheynet[2], Blandine Padey[4,9], Victoria Duliere[4,10], Thomas Julien[4,10], Stéphane Paul[4], Paul Bastard[11,12,13], Alexandre Belot[3,4], Antonin Bal[5,6], Jean-Laurent Casanova[11,12,13,14], Manuel Rosa-Calatrava[4,10], Florence Morfin[5,6], Thierry Walzer[4], and Sophie Trouillet-Assant[4]

IFN-I and IFN-III immunity in the nasal mucosa is poorly characterized during SARS-CoV-2 infection. We analyze the nasal IFN-I/III signature, namely the expression of ISGF-3–dependent IFN-stimulated genes, in mildly symptomatic COVID-19 patients and show its correlation with serum IFN-α_2 levels, which peak at symptom onset and return to baseline from day 10 onward. Moreover, the nasal IFN-I/III signature correlates with the nasopharyngeal viral load and is associated with the presence of infectious viruses. By contrast, we observe low nasal IFN-I/III scores despite high nasal viral loads in a subset of critically ill COVID-19 patients, which correlates with the presence of autoantibodies (auto-Abs) against IFN-I in both blood and nasopharyngeal mucosa. In addition, functional assays in a reconstituted human airway epithelium model of SARS-CoV-2 infection confirm the role of such auto-Abs in abrogating the antiviral effects of IFN-I, but not those of IFN-III. Thus, IFN-I auto-Abs may compromise not only systemic but also local antiviral IFN-I immunity at the early stages of SARS-CoV-2 infection.

Introduction

Cell-intrinsic immunity starts with microbial detection through innate sensors. In case of infection by RNA viruses such as SARS-CoV-2, the sensing may involve cytosolic retinoic acid–inducible gene I, melanoma differentiation-associated protein 5 (Schultze and Aschenbrenner, 2021), and endosomal TLR3 (Gao et al., 2021). The activation of these receptors triggers a signaling cascade that leads to the induction of type I and III IFNs (IFN-I and IFN-III). During the early phase of this cascade, the transcription of different IFN-I and IFN-III genes and numerous IFN-stimulated genes (ISGs) is induced. Secreted IFN-I binds to IFN receptors that signal through JAK1 and tyrosine kinase 2 and activate STAT1, STAT2, and IFN regulatory factor 9. The last three then form a complex called ISGF-3 that translocates to the nucleus and binds to IFN-stimulated response elements (ISREs), thereby inducing the expression of hundreds of ISGs, most of which have antiviral activity. Secreted IFN-III binds to another receptor complex composed of IFNLR and IL10RB and activates the same ISGF-3 complex, inducing the expression of a large number of overlapping ISGs (Lazear et al., 2019). ISGF-3 may also participate to the induction of ISGs downstream IFN-II

[1]Molecular biology core facility, Civils Hospices of Lyon, Lyon Sud Hospital, Pierre-Bénite, France; [2]Joint Research Unit Civils Hospices of Lyon-bioMérieux, Civils Hospices of Lyon, Lyon Sud Hospital, Pierre-Bénite, France; [3]Open Innovation & Partnerships, bioMérieux S.A., Marcy l'Etoile, France; [4]International Center of Research in Infectiology, Institut National de la Santé et de la Recherche Médicale U1111, Centre National de la Recherche Scientifique UMR5308, École normale supérieure Lyon, Claude Bernard Lyon 1 University, Lyon, Rhône, France; [5]Intensive Care Medicine, Croix-Rousse hospital, Claude Bernard Lyon 1 University, Lyon, France; [6]Virology laboratory, Institute of Infectious Agents, Laboratory associated with the National Reference Centre for Respiratory Viruses, Civils Hospices of Lyon, Lyon, France; [7]Occupational Health and Medicine Department, Hospices Civils de Lyon, Lyon, France; [8]Université Claude Bernard Lyon 1, Institut français des sciences et technologies des transports, de l'aménagement et des reseaux, Unité Mixte de Recherche Epidémiologique et de Surveillance Transport Travail Environnement, UMR T_9405, Lyon University, Lyon, France; [9]Signia Therapeutics SAS, Lyon, France; [10]VirNext, Faculty of Medicine RTH Laennec, Claude Bernard Lyon 1 University, Lyon University, Lyon, France; [11]Laboratory of Human Genetics of Infectious Diseases, Necker Branch, Institut National de la Santé et de la Recherche Médicale U1163, Necker Hospital for Sick Children, Paris, France; [12]University of Paris, Imagine Institute, Paris, France; [13]St. Giles Laboratory of Human Genetics of Infectious Diseases, Rockefeller Branch, The Rockefeller University, New York, NY; [14]Howard Hughes Medical Institute, New York, NY.

*J. Lopez, M. Mommert, W. Mouton, A. Pizzorno, and K. Brengel-Pesce contributed equally to this paper; Correspondence to Thierry Walzer: thierry.walzer@inserm.fr; Sophie Trouillet-Assant: sophie.assant@chu-lyon.fr

On behalf of the Lyon COVID study group (Jimmy Perrot, Isabelle Mosnier, Kahina Saker, Guy Oriol, Sylvie Pons, Alexandre Gaymard, Laurence Generenaz, Sylvie Pillet, Bruno Pozzetto, Quentin Lebon, Virginie Pitiot, and Audrey Guichard).

(Platanitis et al., 2019) but is not essential for IFN-γ–dependent immunity (Rosain et al., 2019).

IFN-I and IFN-III participate in the first line of defense against infection, as they promote virus clearance, induce tissue repair, and stimulate the adaptive immune response. However, IFN-I activity has been reported at very low or undetectable levels in the blood (Hadjadj et al., 2020; Trouillet-Assant et al., 2020b) and the nasal epithelium (Ziegler et al., 2021) of some critically ill COVID-19 patients. This defect is explained in some patients by inborn genetic defects of IFN-I induction or amplification (Zhang et al., 2020b) and in others by the presence of neutralizing autoantibodies (auto-Abs) against type I IFNs, mainly IFN-α and/or IFN-ω and, in rare cases, IFN-β (Bastard et al., 2020). These auto-Abs underlie life-threatening pneumonia in at least 10% of intensive care unit (ICU)–admitted COVID-19 patients, as reported by multiple independent cohort studies (Zhang et al., 2020b; Bastard et al., 2020; Troya et al., 2021; Koning et al., 2021; van der Wijst et al., 2021 *Preprint*). While IFN-I immunity is essential for pulmonary immunity to SARS-CoV-2, the contribution of IFN-III immunity remains unknown.

The delayed production of IFN-I is thought to result in unbalanced immune responses unable to clear the virus (Channappanavar et al., 2016; Carvalho et al., 2021; Blanco-Melo et al., 2020). A two-step model of pathogenesis has proposed that insufficient IFN-I levels and hence insufficient ISGs induction during the first 10 d of infection underly viral spread, thereby accounting for the subsequent pulmonary and systemic inflammation that is characteristic of critical cases in which leukocytes attempt to resolve what IFN-I did not in the first place (Zhang et al., 2020a). However, few studies have performed longitudinal measurements of immunity during the acute phases of infection, especially in mildly symptomatic individuals, and thus the dynamics of IFN-I activity relative to virus infection and other immunological perturbations remains largely elusive. Moreover, early host–pathogen interactions occurring at the primary infection site (i.e., the nasal mucosa) are likely to influence in a major way the clinical outcome of infection (Robinot et al., 2021). While many studies have characterized the systemic immune response against SARS-CoV-2, little is known about the immune events occurring in the nasopharyngeal (NP) mucosa. Two recent RNA-sequencing studies have reported ISGs induction in the nasal mucosa of mildly symptomatic COVID-19 patients at diagnosis (Mick et al., 2020; Ng et al., 2021), but whether or how this induction correlates with viral parameters, the dynamics of the peripheral immune response, the delay after symptom onset, and the clinical outcome remains unclear. Moreover, epithelial cells specifically express the IFN-λ (IFN-III) receptor. This receptor signals through a similar JAK-STAT pathway as the IFN-I receptor complex and induces many of the same ISGs that are regulated by the binding of ISGF-3 to ISREs (Schneider et al., 2014), and both IFN-I and IFN-III can restrict SARS-CoV-2 infection of human airway epithelial cultures (Vanderheiden et al., 2020). However, the relative contributions of IFN-I and IFN-III in the defense against SARS-CoV-2 infection in vivo remain unknown. Here, we set out to fill these gaps in knowledge by studying in parallel mucosal and systemic immunity in COVID-19 patients using different RNA-based technologies and comparing patients with and without auto-Abs neutralizing IFN-I.

Table 1. **Demographic and clinical characteristics of health care workers with mild COVID-19 symptoms and critically ill COVID-19 patients**

	Mild COVID-19 (n = 44)	Critically ill COVID-19 (n = 26)
Demographics		
Age (yr), median [IQR]	38.0 [28.8–48.0]	56.5 [54.0–68.0]
Sex		
Male, *n* (%)	5 (11)	19 (73)
Female, *n* (%)	39 (89)	7 (27)
BMI (kg/m²), median [IQR]	23.9 [22.4–26.3]	30.2 [27.1–34.2]
Clinical characteristics		
Delay between symptom onset and ICU admission (days), median [IQR]	N/A	8.0 [6.0–11.8]
ICU length of stay (days), median (minimum-maximum)	N/A	11.5 (3-69)
Mortality, *n* (%)	N/A	8 (31)

All laboratory data were recorded at recipient inclusion. BMI, body mass index; IQR, interquartile range; N/A, not applicable.

Results

Blood IFN-I activity is high at diagnosis and correlates with viral load in mildly symptomatic COVID-19 patients

We aimed to study the dynamics of nasal and blood transcriptome in patients during SARS-CoV-2 infection. For this purpose, we constituted a cohort of health care workers presenting mild COVID-19 symptoms (n = 44 patients; Trouillet-Assant et al., 2020a) and no respiratory coinfection and for whom the delay between symptom onset and SARS-CoV-2 molecular screening was ≤7 d (Table 1). We collected blood samples and nasal swabs weekly for 4 wk, starting at diagnosis (four different visits [V1–V4]; see Fig. S1, which outlines the study); a group of uninfected healthy controls (HCs) was also included (n = 5). We first measured the transcript levels of 800 genes associated with different immune pathways in blood cells using the NanoString technology ("host response" panel). We compared changes in gene expression between mildly symptomatic patients at each time point of the study (V1–V4) and HCs in order to identify differentially expressed genes (DEGs; Table S2). Most changes in gene expression were found at V1 (i.e., at diagnosis of COVID-19; Fig. S2 A). A principal-component analysis confirmed this result and additionally showed that all patients at V3 and V4 and two thirds of patients at V2 grouped together with HCs, while one third of V2 samples clustered between V1 and the other samples (Fig. 1 A). Thus, changes in gene expression in leukocytes mainly occurred before seroconversion, which generally occurs between V1 and V2 (Fig. S2 B). The top functional pathways associated with DEG at V1 according to the nSolver NanoString analysis software were ISGs, including IFN-I– and

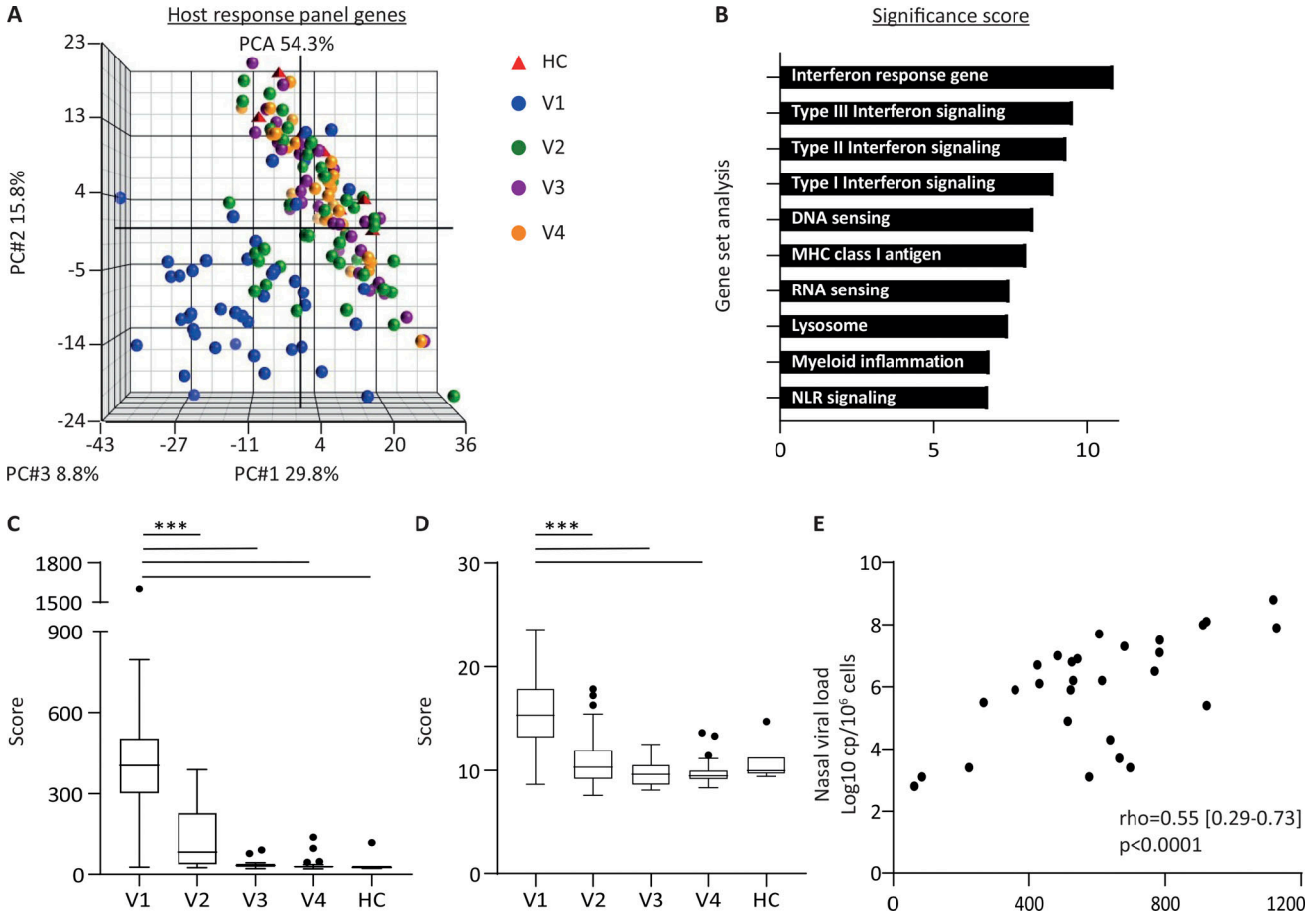

Figure 1. **SARS-CoV-2 infection leads to a transient and acute type I/III IFN signature in the blood. (A)** Principal-component analysis (PCA) of NanoString host response gene expression data from blood of 5 HC (red triangles) and 44 COVID-19 patients (spheres) followed longitudinally from diagnosis (V1, blue) for 4 wk (V2, green; V3, purple; and V4, orange). The percentage of variance captured by each principal-component (PC) axis is indicated, as well as the total variance. The vector position for each sample was plotted and the visualization was performed using Genomics Suite 7 (Partek). **(B)** Pathway analysis for the 123 DEGs between V1 and V2/V3/V4 determined using nSolver NanoString analysis software. The significance scores for the top 10 pathways are indicated. NLR, nucleotide oligomerization domain–like receptor. **(C and D)** Box and whisker plots (using the Tukey method) showing the expression score of the indicated pathways from V1 to V4 for patients and for HCs. A Kruskal–Wallis with uncorrected Dunn's test was used for statistical analysis of data presented in this figure (multiple comparisons; ***, P < 0.001). **(E)** Correlation between the nasal SARS-CoV-2 normalized viral load and the NanoString IFN score (49 genes differentially expressed between V1 and V2/V3/V4). The Spearman's correlation coefficient is shown.

IFN-III–dependent ISGs (i.e., ISGs driven by ISGF-3 binding to ISRE) and IFN-II–dependent ISGs (i.e., ISGs mainly driven by γ-activated factor binding to gamma IFN activation sites; Fig. 1 B). To monitor the representation of these pathways in a longitudinal manner, we computed an expression score based on the combined expression of different ISGs (see Materials and methods). As shown in Fig. 1, C and D, the type I/III ISGs (ISG-I/III) and ISG-II scores were maximal at V1 and lower for other time points, even though they were still significantly higher at V2 compared with HC samples. Moreover, other pathways were significantly enriched at V1, including DNA/RNA sensing, MHC-I antigen presentation, lysosome, myeloid inflammation, and nucleotide oligomerization domain–like receptor signaling; for all these pathways, the scores were significantly higher at V1 compared with HCs and similar between other time points and HCs (Fig. S3). The ISG-I/III score at V1 was associated with the normalized viral load determined at diagnosis (Fig. 1 E; Spearman ρ = 0.55, P < 0.0001), but not with age, body mass index, or delay after symptoms (Fig. S2 C). Altogether, these data highlight the predominance of ISGs among the genes induced in blood cells in response to SARS-CoV-2 infection, the transient nature of this induction, and its association with viral load.

Coordinated regulation of nasal and blood ISGs in response to IFN-I during infection

Next, we aimed to study the regulation and the role of IFN-I/III signaling in the nasal mucosa in response to SARS-CoV-2 infection. For this, we took advantage of the nasal swabs used for standard molecular SARS-CoV-2 screening. However, measuring the host response in such samples is technically challenging, as the amount of cellular material is extremely limited. To overcome this problem, we used the FilmArray technology, a nested PCR-based technique allowing rapid and sensitive measurement of ISGs transcripts that has been recently described (Mommert et al., 2021) and that we adapted for nasal swabs. This technique is advantageous, as it is semiautomated and also

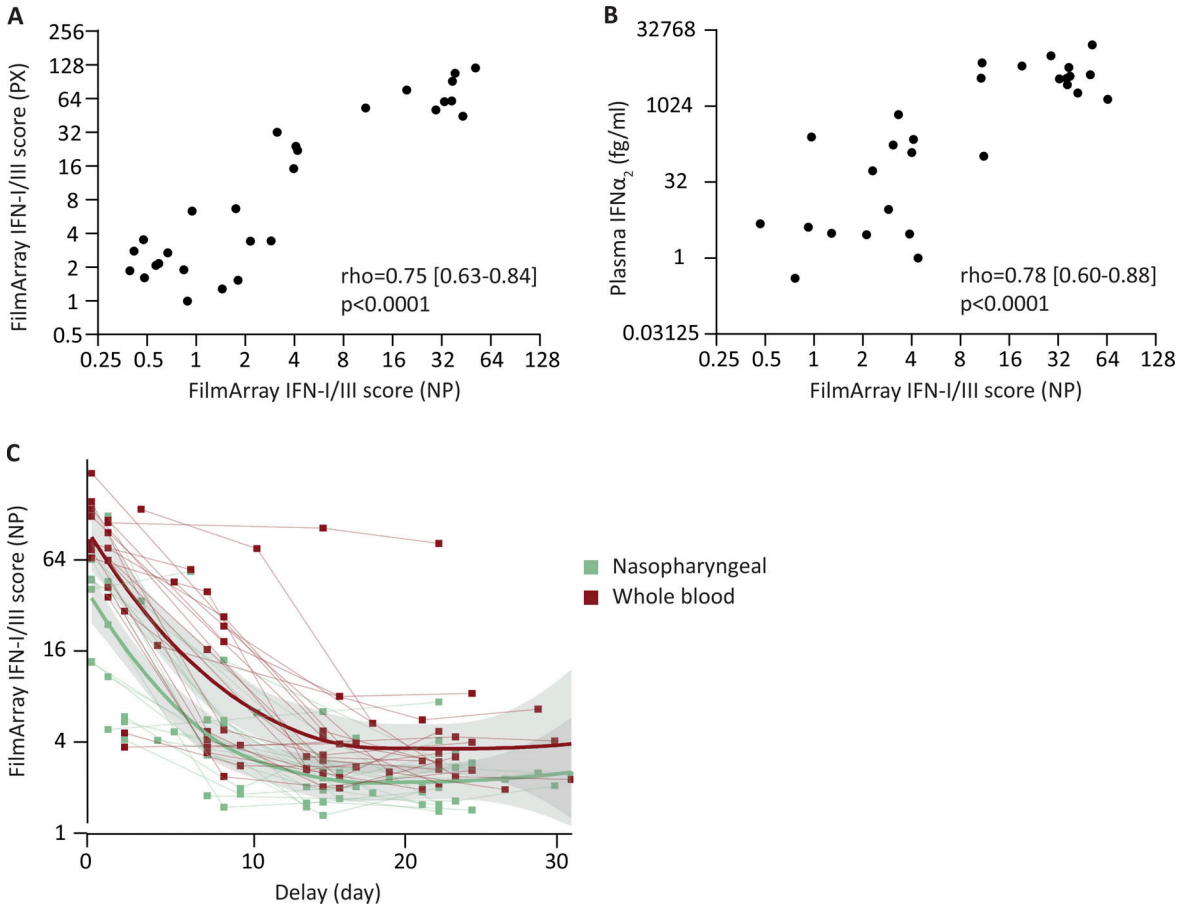

Figure 2. **Nasal and blood IFN-I/III scores are correlated during SARS-CoV-2 infection.** The NP IFN-I/III (IFN) score, defined by a four-ISGs transcriptional signature measured using FilmArray technology, was evaluated. **(A)** Correlation between the NP IFN-I/III score and the blood IFN-I/III score obtained from the PAXgene whole-blood sample (PX, *n* = 75 longitudinal samples from 23 patients). The Spearman's correlation coefficient is shown. **(B)** Correlation between the IFN-I/III score and IFN-α_2 levels (fg/ml) in plasma (*n* = 39 samples with a detectable value from 23 patients), measured by single-molecule array using a commercial kit. The Spearman's correlation coefficient is shown. **(C)** Kinetic measurements of the NP (green) and blood IFN-I/III scores (red) post COVID-19 diagnosis. *n* = 75 longitudinal samples from 23 patients. Fit Loess curves represent local polynomial regressions as determined by the Loess method. Confidence interval at 95% is indicated (gray area).

designed for clinical routine, providing an IFN-I/III score based on the quantification of four ISGs regulated through ISGF3-dependent ISREs (i.e., *IFI27*, *IFI44L*, *RSAD2*, and *IFIT1*; Hernandez et al., 2018). We monitored the nasal IFN-I/III score at diagnosis in 23 SARS-CoV-2–infected health care workers and compared this score with the blood IFN-I/III score and the serum level of IFN-α_2 from the same patients. There was a strong correlation between nasal and blood IFN-I/III scores (Fig. 2 A) and between the nasal IFN-I/III score and serum IFN-α_2 levels (Fig. 2 B; Spearman $\rho > 0.75$ for both comparisons). We also measured the serum level of IFN-λ_1, even though this cytokine is believed to act in a local manner (Park and Iwasaki, 2020). IFN-λ_1 was detectable in the serum of many patients, and its levels were also correlated with the nasal and blood IFN-I/III scores, but the correlation coefficient for these relations was lower than those of IFN-α_2 and IFN-I/III scores (Fig. S4). We then compared the dynamics of the IFN-I/III score in the blood versus nasal mucosa, taking advantage of the availability of serial and paired blood samples and nasal swabs. Both parameters followed very similar kinetics, peaking at the earliest time points after symptom onset and rapidly decreasing thereafter, becoming virtually negative 14 d after symptom onset (Fig. 2 C). This overlap confirms the coordination of nasal and systemic IFN-I/III antiviral defenses and shows that the nasal IFN-I/III score measured using FilmArray directly from swab samples is a faithful proxy of the blood IFN-I/III score in patients.

The nasal IFN-I/III score is correlated with the nasal SARS-CoV-2 load and virus infectivity

Next, we examined the possibility of using the nasal IFN-I/III score as a biomarker of SARS-CoV-2 infection when combined with SARS-CoV-2 RT-PCR. To this aim, we first tested the association between the nasal SARS-CoV-2 viral load and the nasal ISG-I/III score, both determined longitudinally and paired for each time point. There was a significant correlation between both parameters (Spearman $\rho = 0.59$ [0.42; 0.73], $P < 0.0001$; Fig. 3 A). Additionally, based on iterative comparisons, we found that a nasal viral load of 4.40 $\log_{10}$ copies [cp]/10^6 cells discriminated best between patients with high and low IFN-I/III scores; accordingly, most patients with viral loads above 4.40 $\log_{10}$ cp/10^6 cells had high nasal (Fig. 3 B) and blood (Fig. 3 C)

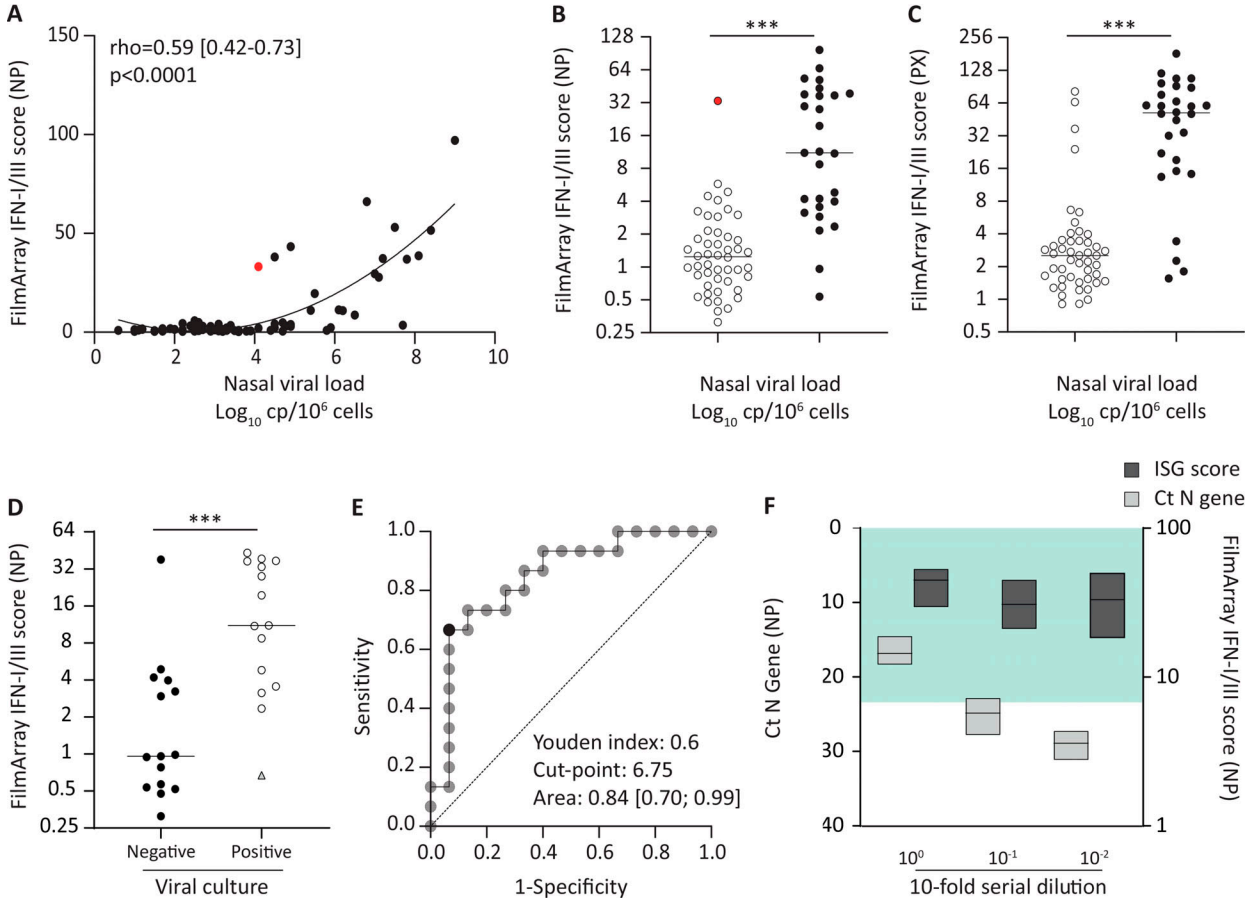

Figure 3. **The nasal IFN-I/III score is a surrogate marker of SARS-CoV-2 infectivity. (A)** Correlation between the NP IFN-I/III (IFN) score and the nasal SARS-CoV-2 normalized viral load (n = 75 longitudinal samples from 23 patients) measured using the SARS-CoV-2 R-gene kit. The Spearman's correlation coefficient is shown. Red dot corresponds to a patient with a strong nasal IFN-I/III score at V1 despite a low viral load <4.4 Log10 cp/10^6 cells. **(B and C)** Scatterplots showing nasal (B) and blood (PX, PAXgene; C) IFN-I/III scores in patients with normalized viral load superior or inferior to 4.40 $\log_{10}$ cp/10^6 cells (n = 75 longitudinal samples from 23 patients). Red dot corresponds to a patient with a strong nasal IFN-I/III score at V1 despite a low viral load <4.4 log10 cp/10^6 cells. Statistical comparison was performed using a nonparametric Mann–Whitney test (***, P < 0.001). **(D)** Scatterplot of the NP IFN-I/III score in patients with positive or negative nasal SARS-CoV-2 viral culture (n = 30 longitudinal samples from 12 patients). Filled circles represent negative virus culture samples, empty circles represent positive virus culture sample, and triangle corresponds to a sample positive on cell culture without cytopathic effect. Statistical comparison was performed using a nonparametric Mann–Whitney test (***, P < 0.001). **(E)** Receiver-operating characteristic curve discriminating between positive and negative SARS-CoV-2 viral culture result. Area under the curve and Youden index are calculated and represent the ability of the NP IFN-I/III score to separate positive and negative viral cultures. **(F)** 10-fold serial dilutions (10° to 10^{-2}) of NP swab samples were performed and followed by measurements of IFN-I/III scores (dark gray, FilmArray) and SARS-CoV-2 load (Ct detection, light gray, SARS-CoV-2 R-gene kit). Data are expressed as floating bars (n = 3; mean [min-max]). The green area depicts the cutoff point IFN-I/III score associated with positive viral culture (6.75).

IFN-I/III scores. A few patients had high ISGs scores despite low virus dose and vice versa, which suggests that other parameters than the virus dose, such as genetic variation, could influence ISGs induction upon infection. We then performed virus culture assays directly from nasal swabs in Vero cells as previously described (Bal et al., 2021) in order to evaluate the putative association between the nasal IFN-I/III score and the isolation of infectious virus from the swab. We found that positive virus cultures were usually associated with high median nasal IFN-I/III scores and, reciprocally, that negative cultures were almost always associated with low median IFN-I/III scores (Fig. 3 D). We then evaluated the interest of using the IFN-I/III score as a surrogate biomarker of replicative SARS-CoV-2 infection through a receiver-operating characteristic curve. The area (95% confidence interval) under the receiver-operating characteristic curve was 0.84 (0.7; 0.99), revealing a good performance of the IFN-I/III score to predict the virus replication capacity with a cut-point score at 6.75 (Fig. 3 E). Of note, one patient had a strong nasal IFN-I/III score at V1 (33.2) despite a low viral load <4.4 $\log_{10}$ cp/10^6 cells (in red in Fig. 3, A and B). For this patient, V1 occurred only 1 d after symptom onset (unlike most of the other patients from the cohort), which suggests that the patient was probably in the ascending phase of viral replication at V1. Accordingly, for this patient, the IFN-I/III score remained high at V2 (43.2) and was associated with a high viral load (>4.4 $\log_{10}$ cp/10^6 cells); of note, the viral culture was positive for both V1 and V2 time points. Lastly, to further evaluate the relevance of using the IFN-I/III score as a marker of replicative infection, we performed comparative measurements of the IFN-I/III score and of the viral RNA in conditions of limiting material mimicked by

10-fold serial dilutions of positive swabs. The Ct (cycle threshold) values of the viral PCR rapidly increased upon swab dilutions, while the IFN-I/III scores remained relatively stable and consistently higher than the 6.75 value previously shown to discriminate between swabs containing or not replicative virus (Fig. 3 F). Altogether, our data highlight the relevance of using the nasal IFN-I/III score as a biomarker of active SARS-CoV-2 infection in combination with SARS-CoV-2 RT-PCR and as a tool to probe the mucosal pathogenesis of COVID-19 at the molecular and cellular levels.

The nasal IFN-I/III score is low in patients with neutralizing anti–type I IFN auto-Abs

A fraction of critically ill COVID-19 patients have low or undetectable blood IFN-I levels (Hadjadj et al., 2020; Trouillet-Assant et al., 2020b), which can be due to either inborn errors of IFN-I immunity (Zhang et al., 2020b), the presence of circulating auto-Abs that neutralize IFN-α and IFN-ω, or both (Bastard et al., 2020). These auto-Abs could also theoretically block mucosal IFN-I, but antibodies do not diffuse as well in tissues as they do in the blood (Iwasaki, 2017), and in some situations, they can be sequestrated within the vascular compartment (Chen et al., 2018). We thus tested the relationships among disease severity, the presence of IFN-I auto-Abs, viral load, and nasal IFN-I/III score. We obtained blood and nasal swabs at ICU admission from 26 critically ill patients (Table 1). The presence of neutralizing auto-Abs against IFN-α and IFN-ω in serum was tested using a novel highly sensitive ELISA (Goncalves et al., 2021). We detected IFN-α and/or IFN-ω auto-Abs in the sera of 8 out of 26 critically ill patients and none of the mildly symptomatic patients (Fig. 4). While most patients without IFN-I auto-Abs and a viral load >4.4 $\log_{10}$ cp/10^6 cells had a very high ISGs score (Fig. 4 A), patients with IFN-I auto-Abs had very low nasal IFN-I/III scores, irrespective of viral load, except for three patients who displayed auto-Abs against IFN-α_2 only and for whom we assumed that IFN-ω could compensate the blockade of IFN-α_2. The other five patients had auto-Abs against both IFN-α and IFN-ω (Fig. 4 B) These data suggest that IFN-I auto-Abs could block IFN-I in the nasal mucosa as well, which was tested by assessing the presence of neutralizing IFN-I auto-Abs in nasal swabs in patients for whom serum auto-Abs levels were also determined. Interestingly, nasal IFN-I auto-Abs were detected in half of the patients who had serum auto-Abs (Table S3). This is consistent with their previous detection in a bronchoalveolar lavage (de Prost et al., 2021). The serum level of IFN-I auto-Abs was not correlated to that of the swab, but differences in the quality of the swab may explain this discrepancy.

Thus, our data suggest that (1) IFN-I is the main inducer of strong ISGs responses in the nasal mucosa, while IFN-III seems insufficient; (2) IFN-I auto-Abs compromise early antiviral defenses in the nasal mucosa of critically ill patients, especially when auto-Abs against both IFN-α_2 and IFN-ω are present; and (3) IFN-ω is involved in nasal IFN-I immunity.

IFN-I auto-Abs block the antiviral effects of IFN-I in a human airway epithelium (HAE) model of SARS-CoV-2 infection

To assess the impact of IFN-I auto-Abs in the early defense against SARS-CoV-2 infection in a more direct manner, we used a previously validated (Pizzorno et al., 2020) and predictive reconstituted HAE model of SARS-CoV-2 infection. In this model, HAEs were treated (24 h before and 1 h after infection) with recombinant IFN-α_2 in the presence or absence of pre-pandemic serum from HCs or patients with biallelic loss-of-function variants of AIRE (autoimmune regulator locus). The latter suffer from autoimmune polyendocrine syndrome type 1 (APS-1) and produce a broad range of auto-Abs, including neutralizing IFN-I auto-Abs (Bruserud et al., 2016; Levin, 2006; Meager et al., 2006). This range is very similar to what is found in a subset of patients with life-threatening COVID-19 (Bastard et al., 2020), which allows testing the impact of IFN-I auto-Abs without the confounding effects of anti–SARS-CoV-2 neutralizing Abs. While recombinant IFN-α_2 significantly inhibited viral replication in the presence of serum from individuals without auto-Abs, this antiviral effect was completely abrogated in the presence of neutralizing auto-Abs from APS-1 individuals, as the viral titers were comparable to those of the untreated control (Fig. 5, A and B). These results were further confirmed by the reduced transepithelial electric resistance values (Fig. 5 C), which are used as reliable surrogate of epithelium integrity (Pizzorno et al., 2020). By contrast, the APS-1 serum had no effect on viral replication when applied in the absence of IFN-I. The presence of APS-1 serum was also associated with lower IFN-α_2–induced IFN-induced protein 44–like (IFI44L) expression (Fig. 5 D). Moreover, the use of a serum from a non–APS-1 individual with IFN-I auto-Abs not previously infected by SARS-CoV-2 showed the same results as those obtained with the APS-1 serum (Fig. S5), excluding the possibility that other auto-Abs not directed against IFN-I in the APS-1 serum may also influence results in the HAE model.

We then directly compared the antiviral effects and ISGs induction capacity of exogenous IFN-α_2, IFN-β_1, IFN-λ_1, IFN-λ_2, IFN-λ_3, and IFN-ω and the impact of IFN-I auto-Abs on these effects in the HAE model. A high concentration of all recombinant IFNs inhibited viral replication (Fig. 6, A–C) and induced *IFI44L* expression (Fig. 6 D); however, neutralizing auto-Abs abrogated only the effect of IFN-α_2 and IFN-ω and not that of IFN-β_1, IFN-λ_1, IFN-λ_2, or IFN-λ_3 (Fig. 6, A–D). Altogether, these results suggest that in the nasal mucosa of infected patients, IFN-α_2 and IFN-ω have a prominent role in the antiviral response that cannot be compensated by other IFNs, probably not expressed at sufficient levels. Moreover, our results functionally validate the neutralizing activity of IFN-I auto-Abs, which further suggests that those Abs could compromise the nasal IFN-I response in a subset of critically ill patients.

Discussion

We investigated herein anti–SARS-CoV-2 IFN-I immunity in a longitudinal way in patients with mild COVID-19 manifestations. This immunity is not well characterized, as most longitudinal studies have focused on hospitalized patients (Lucas et al., 2020; Liu et al., 2021; Szabo et al., 2021; Bernardes et al., 2020). IFN-I/III ISGs and IFN-II ISGs were the main groups of genes upregulated in the blood during infection. This finding confirms the impact of IFNs in the antiviral immune response, which is

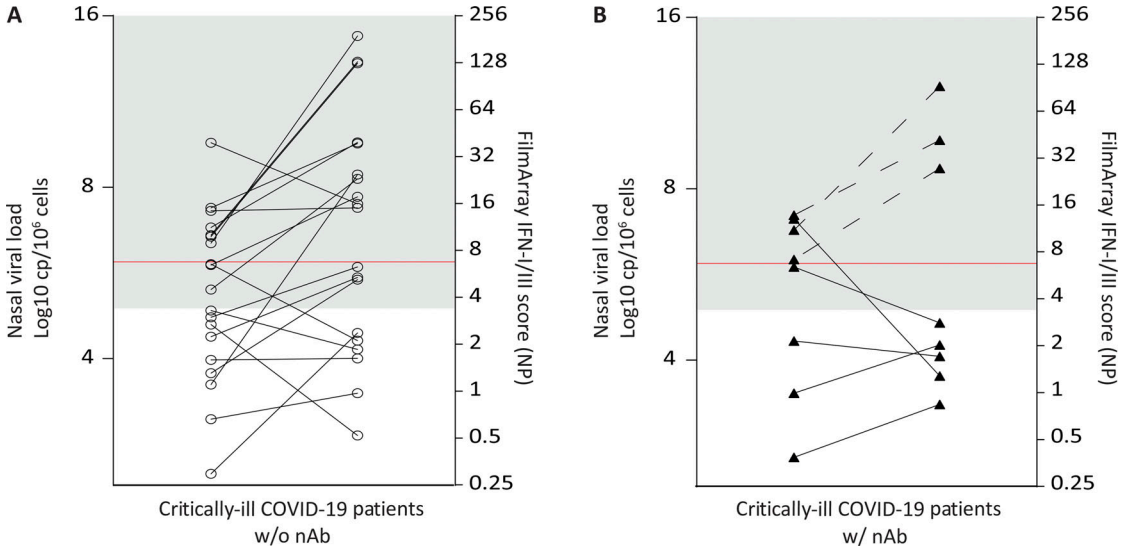

Figure 4. **Critically ill COVID-19 patients with auto-Abs have a weak nasal IFN-I/III score despite high virus load. (A and B)** Comparison of normalized nasal viral load and NP IFN-I/III (IFN) scores in critically ill COVID-19 patients without anti-IFN auto-Abs (A; empty spheres) or with neutralizing auto-Abs (nAb) against IFN-α (B; black triangles). The gray area represents the viral load obtained for 15 out of 17 mildly symptomatic COVID-19 patients (88%) with an IFN-I/III score >6.75 (cutoff value associated with positive viral culture, in red). Dashed lines represent patient with auto-Abs against IFN-α_2 only.

also supported by previous observations according to which severe COVID-19 patients develop auto-Abs against IFN-I or have inborn defects of IFN-I induction, amplification, or response (Bastard et al., 2020). Interestingly, other patients with these inborn defects in IFN-I induction or with auto-Abs against IFN-I are prone to other viral infections, for which there is incomplete penetrance (Bastard et al., 2021b; 2021c; Duncan et al., 2015; Gothe et al., 2020; Hernandez et al., 2019), while the penetrance of COVID-19 critical forms is probably very high. Our data show that in most patients with mild COVID-19, the upregulation of ISGs was transient, maximal at diagnosis, and coordinated with antigen presentation, which presumably helps initiating the ensuing adaptive immune response. The ISGs wave indeed preceded seroconversion, which occurred on average 14 d after symptom onset, consistent with previous studies (Premkumar et al., 2020; Rydyznski Moderbacher et al., 2020).

We showed that the mucosal IFN-I/III signature was correlated with the blood IFN-I signature. Two recent studies have also reported a strong induction of ISGs in the nasal mucosa of SARS-CoV-2–infected patients, which was even higher compared with patients infected with other viruses, such as influenza or seasonal coronaviruses (Mick et al., 2020; Ng et al., 2021), confirming that a high ISGs expression is a hallmark of anti–SARS-CoV-2 mucosal immunity (Pizzorno et al., 2020). Interestingly, another study has also reported that the nasal ISGs expression was higher in pediatric than in adult patients infected with SARS-CoV-2 (Pierce et al., 2021), which could explain the differences in disease severity observed between these two populations. However, the pediatric patients included in the latter study were in fact symptomatic and presenting to the emergency department (Pierce et al., 2021), suggesting that their immune response was not comparable to typically asymptomatically infected children.

Using FilmArray technology, we found that the nasal IFN-I/III score was commensurate to the viral load and to virus infectivity, which is interesting, since SARS-CoV-2 RT-PCR results are often difficult to interpret in clinical routine when Ct values are high and in the absence of clinical manifestation (Han et al., 2021). The nasal ISG-I/III score could therefore be used as a biomarker of active SARS-CoV-2 infection in combination with SARS-CoV-2 RT-PCR to rapidly help in the identification of patients at risk of virus transmission and reciprocally help to avoid quarantine measures in patients who do not or no longer represent a possible source of contamination.

We also found that a sizeable fraction of critically ill patients had a low nasal IFN-I/III score despite a high viral load. These data extend previous findings that the blood IFN-I signature or the serum IFN-I concentration was very low in a subset of critically ill patients (Trouillet-Assant et al., 2020b; Bastard et al., 2020). Thus, the measurement of the nasal IFN-I/III score could be used to help stratify patients and identify patients at risk of developing severe symptoms at early stages of infection. Many COVID-19 therapeutic treatments are currently being tested (for a review, see Canedo-Marroquín et al., 2020), and it is likely that their efficacy will depend on their timely administration during the infection (Park and Iwasaki, 2020), which prompts the identification of early markers of disease severity. We also detected IFN-I auto-Abs in both serum and nasal swabs in a fraction of critically ill patients, in particular in patients with a low nasal IFN-I/III score despite a high viral load. These data suggest that IFN-I auto-Abs could explain the low nasal IFN score in a subset of patients and thus that IFNs-I are the main drivers responsible for inducing protective ISGs signatures in the nasal epithelium compared with IFNs-III. The observation that a few patients with IFN-α_2 auto-Abs without IFN-ω auto-Abs had a high nasal IFN-I/III score suggests a redundancy between IFN-α and IFN-ω in this process. The blockade of IFN-I signaling at the site of virus infection could help virus dissemination by preventing the IFN-I system to render epithelial and

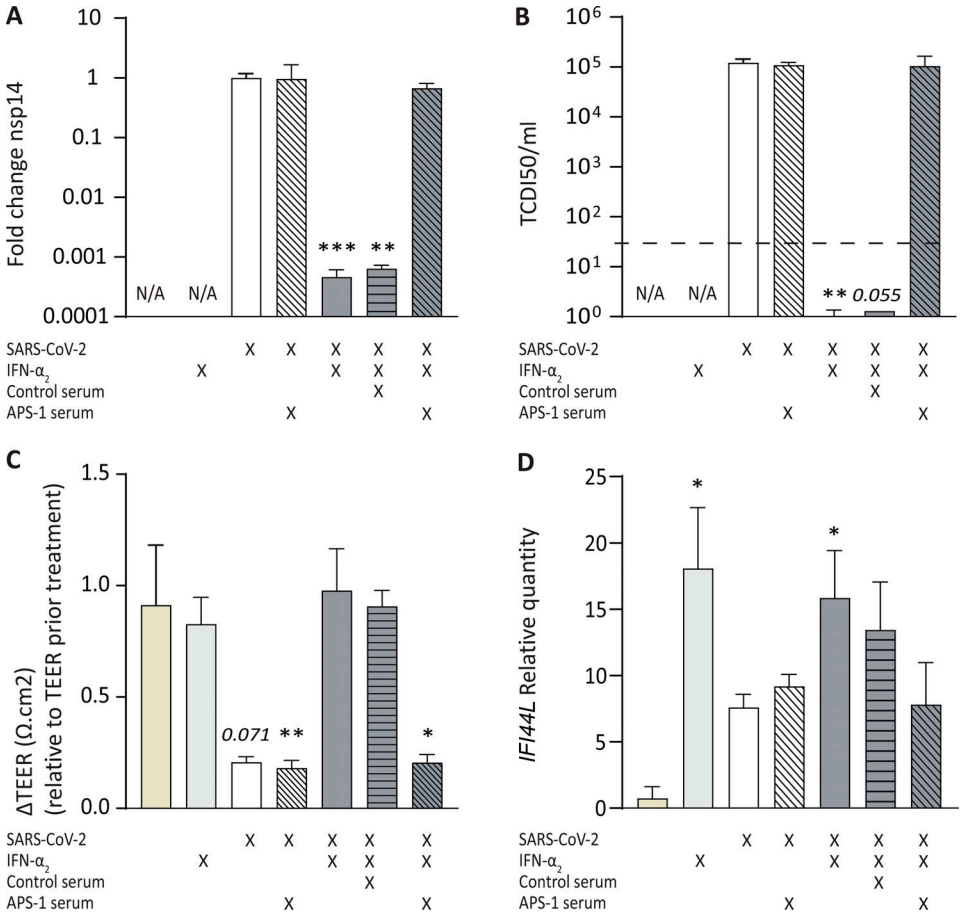

Figure 5. **Sera containing anti–IFN-I antibodies neutralize IFN-α_2 antiviral activity in a reconstituted HAE model of SARS-CoV-2 infection.** The effect of APS-1 serum was evaluated in an HAE model of SARS-CoV-2 infection. **(A)** Nasal HAEs were treated (24 h before and 1 h after SARS-CoV-2 infection) with recombinant IFN-α_2 in the presence or absence of APS-1 patient or control serum, as indicated. Apical washes were performed 54 hpi, and viral titers were determined by RT-PCR. Results are representative of three biological replicates and expressed as relative to the mock-treated control. **(B)** Apical infectious viral titers 54 hpi determined by TCID50 (median tissue culture infectious dose). The dotted line depicts the limit of detection. **(C)** Relative TEER (Δ TEER) between t = 0 and t = 54 hpi. **(D)** Relative expression of *IFI44L* assessed using FilmArray technology from total cellular RNA extracted after infection. In the figure, bars and error bars represent mean and SD, respectively. A Kruskal–Wallis with uncorrected Dunn's test was used for statistical analysis of data presented in this figure (multiple comparisons; *, P < 0.05; **, P <0.01; ***, P < 0.001). In A, B, and D, the reference condition was SARS-CoV-2 alone (white bars), and in C, the reference was the mock condition (beige bars).

other ACE2-expressing cells refractory to infection. We demonstrated this experimentally using a reconstructed epithelium that we infected with SARS-CoV-2 and in which we showed that serum auto-Abs could block the effects of both IFN-α and IFN-ω. A recent study has reported the presence of IFN-I auto-Abs in tracheal aspirates as well (de Prost et al., 2021), suggesting that auto-Abs could block IFN-I signaling at multiple sites. We observed that some critically ill patients had a fairly low viral load despite the presence of anti–IFN-I auto-Abs. This could be explained by later sampling for these patients, associated with a spread of the infection to the lower lungs (Wang et al., 2020).

As recently discussed (Stertz and Hale, 2021), many questions remain, such as how auto-Abs that are produced at modest titers in the serum (Goncalves et al., 2021) block IFN-I at mucosal sites where their diffusion is likely rather limited, even though we detected them in the present study. Moreover, auto-Abs are difficult to manage in clinical practice (de Prost et al., 2021; Bastard et al., 2021a), and it is unclear which therapies should be administered to COVID-19 patients upon detection of IFN-I auto-Abs. Our findings suggest that early therapy with IFN-β, which is apparently not neutralized in most patients with auto-Abs against IFN-I and the response to which is not affected in most patients with inborn defects of IFN-I, may prevent the development of critical disease. An alternative is IFN-III, which displayed antiviral activity in our in vitro system regardless of the presence of IFN-I auto-Abs. Other studies have shown its efficacy in animal models (Park and Iwasaki, 2020). Many clinical trials on the prophylactic and therapeutic use of IFNs for COVID-19 care are ongoing (Sallard et al., 2020) and might bring answers to these questions.

Material and methods

Participants and ethics statement

HC participants

HCs were recruited among donors to the Lyon blood transfusion center (Etablissement Français du Sang) and were considered as

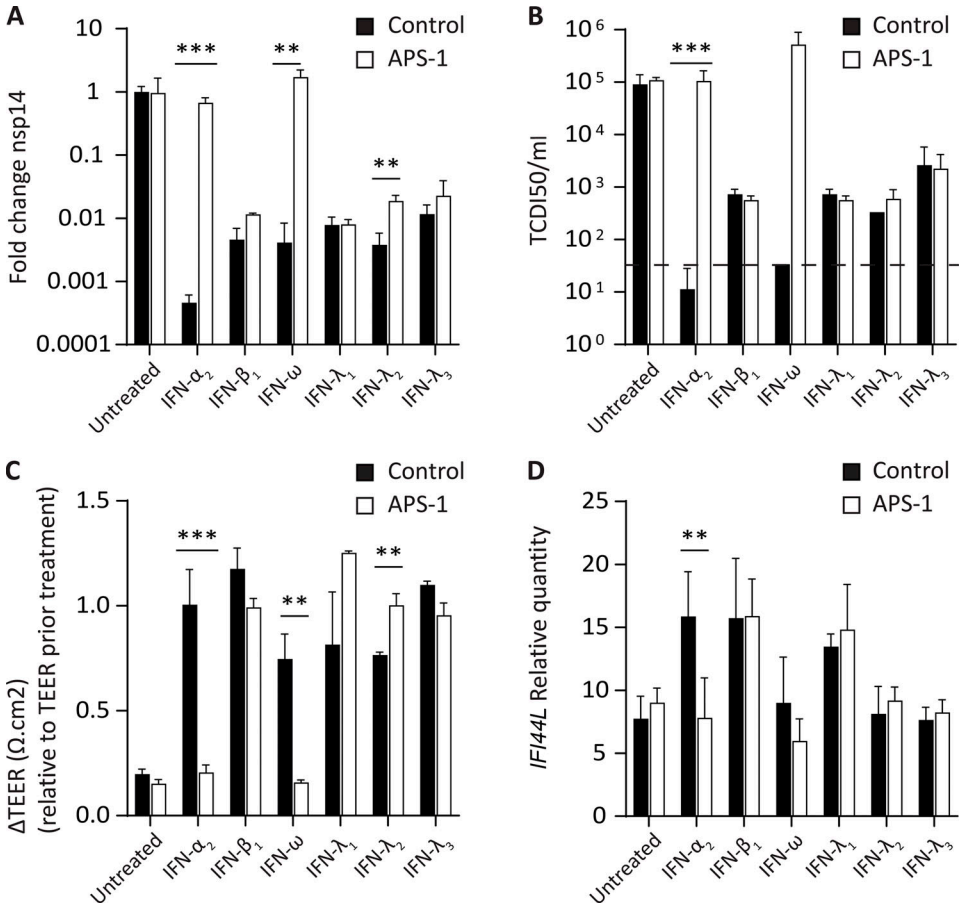

Figure 6. **Sera from APS-1 patients do not influence IFN-β_1, IFN-λ_1, IFN-λ_2, and IFN-λ_3 antiviral activity but block IFN-α and IFN-ω antiviral activity.** The effect of APS-1 serum (white bars) was evaluated in a reconstituted HAE model of SARS-CoV-2 infection in comparison with a control condition (black bars). **(A)** Nasal HAEs were treated (24 h before and 1 h after SARS-CoV-2 infection) with recombinant IFN-α_2, IFN-β_1, IFN-λ_1, IFN-λ_2, IFN-λ_3, or IFN-ω in the presence or absence of APS-1 serum. Apical washes were performed at 54 hpi, and viral titers were determined by RT-PCR. Results are representative of three biological replicates and expressed as relative to the mock-treated control. **(B)** Apical infectious viral titers at 54 hpi determined by TCID50. The dotted line depicts the limit of detection. **(C)** Δ TEER between t = 0 and t = 54 hpi. **(D)** Relative expression of *IFI44L* assessed using FilmArray technology from total cellular RNA extracted after infection. In the figure, bars and error bars represent mean and SD, respectively. Multiple t tests with Bonferroni–Dunn method were used for the statistical analysis of data presented in this figure (comparison between control and APS-1 serum conditions in each readout; **, P < 0.01; ***, P < 0.001).

a control group. According to French procedures, a written nonopposition to the use of donated blood for research purposes was obtained from HCs. The donors' personal data were anonymized before transfer to our research laboratory. We obtained approval from the local ethical committee and the French ministry of research (DC-2008-64) for handling and conservation of these samples.

Mildly symptomatic COVID-19 participants

A prospective longitudinal cohort study was conducted at the Hospices Civils de Lyon (university hospital of Lyon, France) including health care workers aged >18 yr, having given their written consent, accepting a 6-wk follow-up, and displaying at least one of the following symptoms suggestive of a SARS-CoV-2 infection: fever, respiratory symptoms, headache, anosmia, and ageusia (Trouillet-Assant et al., 2020a). Exclusion criteria were being pregnant or lactating. The COVID-19 diagnosis was confirmed by quantitative RT-PCR (Cobas SARS-CoV-2 Test; Roche Diagnostics). The NP swab used were either in Copan Universal Transport Medium or in Cobas PCR medium tube. Clinical and microbiological data were collected for all included health care workers. Patients with a positive RT-PCR result at inclusion (V1) came back weekly (V2, V3, and V4) for blood and NP sampling until negativation (assessed by RT-PCR). Ethics approval was obtained from the national review board for biomedical research in April 2020 (Comité de Protection des Personnes Sud Méditerranée I, Marseille, France; ID RCB 2020-A00932-37), and the clinical study was registered at www.clinicaltrials.gov (NCT04341142, v3).

Critically ill COVID-19 patients

All critically ill patients, admitted to the ICU, were included in the MIR-COVID study. This study was registered to the Commission nationale de l'informatique et des libertés (French national data protection commission) under the number 20–097 and was approved by an ethical committee for biomedical research

(Comité de Protection des Personnes HCL) under the number 20-41. In agreement with the General Data Protection Regulation (Regulation [EU] 2016/679 and Directive 95/46/EC) and the French data protection law (law 78-17 on 06/01/1978 and Décret 2019-536 on 29/05/2019), we obtained consent from each patient or his/her next of kin. During the ICU stay, blood collected on EDTA tubes were used for anti-IFN antibody investigation as previously described. For this study, nasal swabs used for molecular SARS-CoV-2 screening at hospital admission were collected for additional experiments.

Whole-blood transcriptomic assessment

Total RNA was extracted from PAXgene tubes using the Maxwell 16 LEV simplyRNA Blood kit (Promega), following the manufacturer's guidelines. RNA quantity was determined using a Nanodrop (Thermo Fisher Scientific). 200 ng total RNA was hybridized with the nCounter Host Response panel (#LBL-10805-01; NanoString) and counted on an nCounter FLEX platform according to the manufacturer's guidelines. Table S1 provides more information on the panel and the genes measured. Raw counts were normalized using internal positive standards and 12 housekeeping genes. Using ROSALIND NanoString Gene Expression packages (https://rosalind.onramp.bio/), we performed differential expression analysis and gene set analysis with a cutoff at ±1.5-fold change and an adjusted P value < 0.05. Gene expression signatures were generated by summing for each of the 60 signatures encompassed in the panel (LBL-10805-01_nCounter_Host_Reposne_Gene_List annotation file) the normalized counts of each gene divided by the median of expression in the control group. Statistical analysis and graphics were performed using Prism 9 software (https://www.graphpad.com).

FilmArray IFN panel

The first prototype of the IFN pouch encompasses four ISGs (IFN α inducible protein 27, *IFI44L*, IFN-induced protein with tetratricopeptide repeats 1, radical S-adenosyl methionine domain containing 2) and three housekeeping genes (hypoxanthine phosphoribosyltransferase 1, peptidylprolyl isomerase B, and 2,4-dienoyl-CoA reductase 1) for signal normalization. 100 µl PAXgene blood or nasal pharyngeal swab samples was tested using the IFN prototype (Tawfik et al., 2020) according to the manufacturer's instructions. In brief, the pouches were hydrated with the hydration solution supplied with the kit. The PAXgene blood or nasal pharyngeal swab samples were mixed with 800 µl of the sample buffer provided with the kit and directly injected into the pouch and ran on FilmArray 2.0 and FilmArray Torch instruments (BioFire Diagnostics). Results were delivered in <1 h. Using a research version of the instrument, real-time quantification cycle values and post-amplification melt peaks were determined for each assay. The normalized expression values of each assay were then computed using the internal reference genes. The nasal pharyngeal ISGs score was calculated using the same method applied for PAXgene sample as previously described (Pescarmona et al., 2019).

IFN-α and IFN-ω concentration determination

Serum IFN-α_2 concentrations (fg/ml) from plasma were measured by single-molecule array using a commercial kit for IFN-α_2 quantification (Quanterix). The assay was based on a three-step protocol using an HD-1 Analyzer (Quanterix) and required 3 h of processing time from sample to result acquisition (Wilson et al., 2016). Plasma IFN-l concentrations were determined using Meso Scale Discovery U-PLEX platform.

Viral load measurement

The SARS-CoV-2 load was determined from the nasal pharyngeal swabs using SARS-CoV-2 R-gene kit (bioMérieux). Briefly, nucleic acid extraction was performed from 0.2 ml nasal pharyngeal swabs on NUCLISENS easyMAG, and amplification was performed using Bio-Rad CFX96. The viral load was quantified using four internally developed quantification standards (QS1–QS4 at 2.5×10^6, 2.5×10^5, 2.5×10^4, and 2.5×10^3 cp/ml, respectively, of SARS-CoV-2 N gene DNA). These quantification standards were quality checked and quantified using the Nanodrop spectrophotometer (Thermo Fisher Scientific) and Applied Biosystems QuantStudio 3D Digital PCR. In parallel, nasal pharyngeal swabs were tested using the CELL Control R-GENE kit (amplification of the *HPRT1* housekeeping gene) that contains two quantification standards (QS1 at 10^4 cp/µl DNA standard that is 50,000 cells/PCR [i.e., 1.25×10^6 cells/ml in our conditions] and QS2 at 10^3 cp/µl DNA standard that is 5,000 cells/PCR [i.e., 1.25×10^5 cells/ml in our conditions]) to normalize the viral load according to the sampling quality (log10 [(number of SARS-CoV-2 copies per milliliter/number of cells per milliliter) × 10^6 cells per milliliter]).

Viral culture

Viral culture was performed following interim biosafety guidelines established by the World Health Organization [WHO/WPE/GIH/2020.3] from nasal pharyngeal swabs in Universal Transport Medium. RT-PCR–positive nasal pharyngeal swabs were inoculated on confluent Vero cells (ATCC CCL-81) in Eagle's minimum essential media supplemented with 2% penicillin-streptomycin, 1% L-glutamine, and 2% inactivated fetal bovine serum. Plates were incubated at 33°C (which was determined to be the optimal temperature for virus cultures) and 5% CO_2 for 96 h. Cytopathic effects were monitored daily; samples were harvested when positive, while negative samples at 96 h underwent subculture on new plates. Culture supernatants were sampled at 2 h after inoculation, at 96 h, and after an additional 96 h on subculture. RNA from supernatants were extracted by the automated MGISP-960 workstation using MGI Easy Magnetic Beads Virus DNA/RNA Extraction Kit (MGI Tech), and SARS-CoV-2 detection was performed using TaqPath COVID-19 CE-IVD RT-PCR kit on a QuantStudio 5 System (Applied Biosystems and Thermo Fisher Scientific).

Serological investigation

The presence of anti–SARS-CoV-2 antibodies was evaluated using the Wantai Ab assay detecting total antibodies against the receptor-binding domain of the S protein.

The presence of anti–IFN-α_2 antibodies was investigated using a commercially available kit (Thermo Fisher Scientific; Goncalves et al., 2021). The neutralizing capacity of patient sera against IFN-α was then evaluated as previously described (Bastard et al., 2021c).

Viral infection and IFN treatment in reconstituted HAE

MucilAir nasal HAE reconstituted from human primary cells was provided by Epithelix SARL and maintained in air–liquid interphase at 37°C and 5% CO_2 in specific culture medium in Costar Transwell inserts (Corning) according to the manufacturer's instructions. 1 d before infection (d–1), HAEs were mock treated or treated through the basolateral pole with a 2 ng/ml or 20 ng/ml final dilution of recombinant IFN-α_{2a}, IFN-β_1, IFN-λ_1, IFN-λ_2, IFN-λ_3 (PBL Assay Science), or IFN-ω (Merck) in 700 µl MucilAir culture medium. To assess the potential neutralizing effect of anti–IFN-I antibodies, recombinant IFN-α_{2a} was preincubated (37°C, 1 h) before addition to HAE with a 1% final dilution of inactivated (56°C, 30 min) pre–COVID-19-pandemic patient sera, containing or not anti–IFN-α antibodies collected from autoimmune polyendocrinopathy-candidiasis-ectodermal dystrophy patients and HCs, respectively. A third serum, obtained from a non–autoimmune polyendocrinopathy-candidiasis-ectodermal dystrophy patient who tested positive for auto-Abs against type I IFNs, was also used as control. 24 h after IFN treatment (d0) in the presence or not of sera, the apical poles of HAE were gently washed twice with warm OptiMEM medium (GIBCO BRL and Thermo Fisher Scientific) and then infected with a 150 µl dilution of SARS-CoV-2 virus in OptiMEM medium at a multiplicity of infection of 0.1, as previously described (Pizzorno et al., 2020). Basolateral treatment with recombinant IFN (with or without sera) was repeated 1 hpi (hour postinfection) in the same conditions as on d–1. Variations in transepithelial electrical resistance (TEER) were measured using a dedicated volt-ohm meter (EVOM2, Epithelial Volt/Ohm Meter) and expressed in Ohm/cm^2. At 54 hpi, HAE apical poles were washed with warm OptiMEM and collected in two tubes, one for TCID50 viral titration and one for quantification of viral genome by RT-PCR. HAE cells were harvested in RLT buffer (Qiagen), and total RNA was extracted using the RNeasy Mini Kit (Qiagen) for subsequent gene expression analyses.

Statistical analysis

Nonparametric Wilcoxon–Mann–Whitney tests and Spearman's correlation tests were performed for all comparisons, unless otherwise specified. A χ^2 test was performed to analyze contingency tables. To calculate the virus load threshold that better divided patients into two ISGs groups, we used the lowest P value of nonparametric significance test (Wilcoxon rank sum) iteratively applied to the ISGs score, split over normalized nasal viral load thresholds ranging from minimum (0.60) to maximum detected values (9.00) with a step of 0.01. All statistical analyses were conducted using R (the R Foundation; https://www.r-project.org/foundation/, version 3.6.1) and GraphPad Prism 8.3.0 software. A P value of < 0.05 was considered statistically significant. Correlations were only performed on dually detected samples.

Online supplemental material

Fig. S1 is a graphical outline of the study. Fig. S2 shows a heatmap of genes differentially expressed between COVID-19 patients at different time points after symptom onset. It also shows seroconversion relative to time after symptom onset and the relations between the IFN score and clinical or virological parameters. Fig. S3 shows the dynamics of blood expression of transcripts related to different immune pathways during SARS-CoV-2 infection. Fig. S4 shows the correlation between blood IFN-I/III scores and serum IFN-λ_1 levels. Fig. S5 shows the effect of a serum from a non–APS-1 patient containing IFN-I auto-Abs on the antiviral activity of IFN-I in the HAE model of SARS-CoV-2 infection. Table S1 lists all genes whose expression is measured in the host response NanoString panel and functional annotation of these genes. Table S2 lists genes differentially expressed between blood cells in mild COVID-19 patients at diagnosis and blood cells from HCs. Table S3 is a contingency table relative to IFN-α auto-Ab detection from nasal and plasma paired samples from mildly symptomatic and critically ill COVID-19 patients.

Acknowledgments

We thank all patients for their participation. We also thank all personnel of the occupational health and medicine department of Hospices Civils de Lyon who contributed to sample collection. Human biological samples and associated data were obtained from NeuroBioTec (Centre de Ressources Biologiques des Hospices Civils de Lyon, Lyon, France; Biobank BB-0033-00046). We thank Karima Brahami and all members of the Direction de la Recherche Clinique et de l'innovation (Hospices Civils de Lyon) for their reactivity and Emilie Laurent and Cedrine Milesi (VirPath team) for their technical support. The authors would like to thank Hélène Boyer for a helpful review of the manuscript.

T. Walzer's laboratory is supported by the Agence Nationale de la Recherche, the Fondation ARC (équipe labellisée), and the Institut National du Cancer and receives institutional grants from Institut National de la Santé et de la Recherche Médicale, Centre National de la Recherche Scientifique, Claude Bernard Lyon 1 University, and École normale supérieure de Lyon. The VirPath team is supported by REACTing, Institut National de la Santé et de la Recherche Médicale, Centre National de la Recherche Scientifique, the Agence Nationale de la Recherche, and Institut Mérieux (Mérieux Research grant). This study was supported by the Hospices Civils de Lyon and the Fondation des Hospices Civils de Lyon. The Laboratory of Human Genetics of Infectious Diseases is supported by the National Institutes of Health (R01AI088364), the National Center for Advancing Translational Sciences, National Institutes of Health Clinical and Translational Science Award program (UL1 TR001866), an Emergent Ventures Fast Grant, the Mercatus Center at George Mason University, the Fisher Center for Alzheimer's Research Foundation, the Meyer Foundation, the JPB Foundation, the Agence Nationale de la Recherche under the "Investments for the Future" program (ANR-10-IAHU-01), the Integrative Biology of Emerging Infectious Diseases Laboratory of Excellence (ANR-10-LABX-62-IBEID), the French Foundation for Medical Research (EQU201903007798), the French Foundation for Medical Research and Agence Nationale de la Recherche GENCOVID project (ANR-20-COVI-0003), Agence Nationale de la Recherche Nord-Sud (ANRS-COV05), Agence Nationale de la Recherche

AABIFNCOV project (ANR-20-C11-0001), the Square Foundation, Grandir - Fonds de solidarité pour l'enfance, the SCOR Corporate Foundation for Science, the Howard Hughes Medical Institute, the Rockefeller University, the St. Giles Foundation, Institut National de la Santé et de la Recherche Médicale, and the University of Paris.

Author contributions: J. Lopez contributed to conceptualization, data curation, formal analysis, supervision, validation, investigation, visualization, methodology, and writing (original draft). M. Mommert contributed to conceptualization, data curation, formal analysis, validation, investigation, visualization, and methodology. W. Mouton contributed to conceptualization, data curation, formal analysis, validation, investigation, visualization, methodology, and writing (original draft, review and editing). A. Pizzorno contributed to conceptualization, data curation, formal analysis, supervision, validation, investigation, visualization, methodology, and writing (original draft, review and editing). K. Brengel-Pesce contributed to conceptualization, supervision, validation, investigation, and methodology. M. Mezidi contributed resources. J.-B. Fassier contributed resources and contributed to funding acquisition. M. Villard contributed to investigation and methodology. B. Lina contributed to methodology and funding acquisition, J.-C. Richard contributed resources. V. Cheynet contributed to data curation, formal analysis, supervision, validation, and methodology. B. Padey contributed to formal analysis and methodology. V. Duliere contributed to formal analysis and methodology. T. Julien contributed to formal analysis and methodology. S. Paul contributed resource. P. Bastard contributed to conceptualization, formal analysis, validation, investigation, visualization, methodology, and writing (original draft). A. Belot contributed resources and contributed to conceptualization. A. Bal contributed to conceptualization, formal analysis, validation, and methodology. J.-L. Casanova contributed to conceptualization and writing (original draft, review and editing). M. Rosa-Calatrava contributed to methodology and funding acquisition and writing (original draft, review and editing). F. Morfin contributed to conceptualization, data curation, formal analysis, validation, investigation, and methodology. T. Walzer contributed to conceptualization, methodology, investigation, visualization, and writing (original draft, review and editing). S. Trouillet-Assant contributed to conceptualization, resources, funding acquisition, investigation, visualization, methodology, project administration, and writing (original draft, review and editing).

Disclosures: M. Mommert, W. Mouton, K. Brengel-Pesce, A. Bal, and V. Cheynet reported personal fees from bioMérieux during the conduct of the study and personal fees from bioMérieux outside the submitted work. M. Mommert, K. Brengel-Pesce, and S. Trouillet-Assant have a patent to FR2107421 pending. A. Pizzorno, B. Padey, and M. Rosa-Calatrava reported a patent to FR 20/02351 (Therapeutic treatments against SARS-CoV-2) pending. S. Trouillet-Assant and J.-B. Fassier reported non-financial support from bioMérieux during the conduct of the study and non-financial support from bioMérieux outside the submitted work. No other disclosures were reported.

Submitted: 3 June 2021
Revised: 17 July 2021
Accepted: 20 July 2021

References

Bal, A., M.-A. Trabaud, J.-B. Fassier, M. Rabilloud, K. Saker, C. Langlois-Jacques, N. Guibert, A. Paul, D. Alfaiate, A. Massardier-Pilonchery, et al. COVID SER Study Group. 2021. Six-month antibody response to SARS-CoV-2 in healthcare workers assessed by virus neutralization and commercial assays. *Clin. Microbiol. Infect.* 27:933–935. https://doi.org/10.1016/j.cmi.2021.01.003

Bastard, P., L.B. Rosen, Q. Zhang, E. Michailidis, H.-H. Hoffmann, Y. Zhang, K. Dorgham, Q. Philippot, J. Rosain, V. Béziat, et al. COVID Human Genetic Effort. 2020. Autoantibodies against type I IFNs in patients with life-threatening COVID-19. *Science.* 370:eabd4585. https://doi.org/10.1126/science.abd4585

Bastard, P., R. Lévy, S. Henriquez, C. Bodemer, T.-A. Szwebel, and J.-L. Casanova. 2021a. Interferon-β Therapy in a Patient with Incontinentia Pigmenti and Autoantibodies against Type I IFNs Infected with SARS-CoV-2. *J. Clin. Immunol.* 41:931–933. https://doi.org/10.1007/s10875-021-01023-5

Bastard, P., J. Manry, J. Chen, J. Rosain, Y. Seeleuthner, O. AbuZaitun, L. Lorenzo, T. Khan, M. Hasek, N. Hernandez, et al. 2021b. Herpes simplex encephalitis in a patient with a distinctive form of inherited IFNAR1 deficiency. *J. Clin. Invest.* 131:e139980. https://doi.org/10.1172/JCI139980

Bastard, P., E. Michailidis, H.-H. Hoffmann, M. Chbihi, T. Le Voyer, J. Rosain, Q. Philippot, Y. Seeleuthner, A. Gervais, M. Materna, et al. 2021c. Autoantibodies to type I IFNs can underlie adverse reactions to yellow fever live attenuated vaccine. *J. Exp. Med.* 218:e20202486. https://doi.org/10.1084/jem.20202486

Bernardes, J.P., N. Mishra, F. Tran, T. Bahmer, L. Best, J.I. Blase, D. Bordoni, J. Franzenburg, U. Geisen, J. Josephs-Spaulding, et al. Deutsche COVID-19 Omics Initiative (DeCOI). 2020. Longitudinal Multi-omics Analyses Identify Responses of Megakaryocytes, Erythroid Cells, and Plasmablasts as Hallmarks of Severe COVID-19. *Immunity.* 53:1296–1314.e9. https://doi.org/10.1016/j.immuni.2020.11.017

Blanco-Melo, D., B.E. Nilsson-Payant, W.-C. Liu, S. Uhl, D. Hoagland, R. Møller, T.X. Jordan, K. Oishi, M. Panis, D. Sachs, et al. 2020. Imbalanced Host Response to SARS-CoV-2 Drives Development of COVID-19. *Cell.* 181:1036–1045.e9. https://doi.org/10.1016/j.cell.2020.04.026

Bruserud, Ø., B.E. Oftedal, N. Landegren, M.M. Erichsen, E. Bratland, K. Lima, A.P. Jørgensen, A.G. Myhre, J. Svartberg, K.J. Fougner, et al. 2016. A Longitudinal Follow-up of Autoimmune Polyendocrine Syndrome Type 1. *J. Clin. Endocrinol. Metab.* 101:2975–2983. https://doi.org/10.1210/jc.2016-1821

Canedo-Marroquín, G., F. Saavedra, C.A. Andrade, R.V. Berrios, L. Rodríguez-Guilarte, M.C. Opazo, C.A. Riedel, and A.M. Kalergis. 2020. SARS-CoV-2: Immune Response Elicited by Infection and Development of Vaccines and Treatments. *Front. Immunol.* 11:569760. https://doi.org/10.3389/fimmu.2020.569760

Carvalho, T., F. Krammer, and A. Iwasaki. 2021. The first 12 months of COVID-19: a timeline of immunological insights. *Nat. Rev. Immunol.* 21:245–256. https://doi.org/10.1038/s41577-021-00522-1

Channappanavar, R., A.R. Fehr, R. Vijay, M. Mack, J. Zhao, D.K. Meyerholz, and S. Perlman. 2016. Dysregulated Type I Interferon and Inflammatory Monocyte-Macrophage Responses Cause Lethal Pneumonia in SARS-CoV-Infected Mice. *Cell Host Microbe.* 19:181–193. https://doi.org/10.1016/j.chom.2016.01.007

Chen, C.-C., E. Pouliquen, A. Broisat, F. Andreata, M. Racapé, P. Bruneval, L. Kessler, M. Ahmadi, S. Bacot, C. Saison-Delaplace, et al. 2018. Endothelial chimerism and vascular sequestration protect pancreatic islet grafts from antibody-mediated rejection. *J. Clin. Invest.* 128:219–232. https://doi.org/10.1172/JCI93542

de Prost, N., P. Bastard, R. Arrestier, S. Fourati, M. Mahévas, S. Burrel, K. Dorgham, G. Gorochov, Y. Tandjaoui-Lambiotte, I. Azzaoui, et al. 2021. Plasma Exchange to Rescue Patients with Autoantibodies Against Type I Interferons and Life-Threatening COVID-19 Pneumonia. *J. Clin. Immunol.* 41:536–544. https://doi.org/10.1007/s10875-021-00994-9

Duncan, C.J.A., S.M.B. Mohamad, D.F. Young, A.J. Skelton, T.R. Leahy, D.C. Munday, K.M. Butler, S. Morfopoulou, J.R. Brown, M. Hubank, et al. 2015. Human IFNAR2 deficiency: Lessons for antiviral immunity. *Sci. Transl. Med.* 7:307ra154. https://doi.org/10.1126/scitranslmed.aac4227

Gao, D., M.J. Ciancanelli, P. Zhang, O. Harschnitz, V. Bondet, M. Hasek, J. Chen, X. Mu, Y. Itan, A. Cobat, et al. 2021. TLR3 controls constitutive IFN-β antiviral immunity in human fibroblasts and cortical neurons. *J. Clin. Invest.* 131:e134529. https://doi.org/10.1172/JCI134529

Goncalves, D., M. Mezidi, M. Perret, K. Saker, N. Fabien, R. Pescarmona, C. Lombard, T. Walzer, J.L. Casanova, A. Belot, et al. 2021. Antibodies against type-I Interferon: detection and association with severe clinical outcome in COVID-19 patients. *Clin. Transl. Immunology*. In press.

Gothe, F., C.F. Hatton, L. Truong, Z. Klimova, V. Kanderova, M. Fejtkova, A. Grainger, V. Bigley, J. Perthen, D. Mitra, et al. 2020. A novel case of homozygous IFNAR1 deficiency with haemophagocytic lymphohistiocytosis. *Clin. Infect. Dis.*:ciaa1790. https://doi.org/10.1093/cid/ciaa1790

Hadjadj, J., N. Yatim, L. Barnabei, A. Corneau, J. Boussier, N. Smith, H. Péré, B. Charbit, V. Bondet, C. Chenevier-Gobeaux, et al. 2020. Impaired type I interferon activity and inflammatory responses in severe COVID-19 patients. *Science.* 369:718–724. https://doi.org/10.1126/science.abc6027

Han, M.S., J.-H. Byun, Y. Cho, and J.H. Rim. 2021. RT-PCR for SARS-CoV-2: quantitative versus qualitative. *Lancet Infect. Dis.* 21:165. https://doi.org/10.1016/S1473-3099(20)30424-2

Hernandez, N., I. Melki, H. Jing, T. Habib, S.S.Y. Huang, J. Danielson, T. Kula, S. Drutman, S. Belkaya, V. Rattina, et al. 2018. Life-threatening influenza pneumonitis in a child with inherited IRF9 deficiency. *J. Exp. Med.* 215:2567–2585. https://doi.org/10.1084/jem.20180628

Hernandez, N., G. Bucciol, L. Moens, J. Le Pen, M. Shahrooei, E. Goudouris, A. Shirkani, M. Changi-Ashtiani, H. Rokni-Zadeh, E.H. Sayar, et al. 2019. Inherited IFNAR1 deficiency in otherwise healthy patients with adverse reaction to measles and yellow fever live vaccines. *J. Exp. Med.* 216: 2057–2070. https://doi.org/10.1084/jem.20182295

Iwasaki, A. 2017. Immune Regulation of Antibody Access to Neuronal Tissues. *Trends Mol. Med.* 23:227–245. https://doi.org/10.1016/j.molmed.2017.01.004

Koning, R., P. Bastard, J.-L. Casanova, M.C. Brouwer, and D. van de Beek. with the Amsterdam U.M.C. COVID-19 Biobank Investigators. 2021. Autoantibodies against type I interferons are associated with multi-organ failure in COVID-19 patients. *Intensive Care Med.* 47:704–706. https://doi.org/10.1007/s00134-021-06392-4

Lazear, H.M., J.W. Schoggins, and M.S. Diamond. 2019. Shared and Distinct Functions of Type I and Type III Interferons. *Immunity.* 50:907–923. https://doi.org/10.1016/j.immuni.2019.03.025

Levin, M. 2006. Anti-interferon auto-antibodies in autoimmune polyendocrinopathy syndrome type 1. *PLoS Med.* 3:e292. https://doi.org/10.1371/journal.pmed.0030292

Liu, C., A.J. Martins, W.W. Lau, N. Rachmaninoff, J. Chen, L. Imberti, D. Mostaghimi, D.L. Fink, P.D. Burbelo, K. Dobbs, et al. COVID Clinicians. 2021. Time-resolved systems immunology reveals a late juncture linked to fatal COVID-19. *Cell.* 184:1836–1857.e22. https://doi.org/10.1016/j.cell.2021.02.018

Lucas, C., P. Wong, J. Klein, T.B.R. Castro, J. Silva, M. Sundaram, M.K. Ellingson, T. Mao, J.E. Oh, B. Israelow, et al. Yale IMPACT Team. 2020. Longitudinal analyses reveal immunological misfiring in severe COVID-19. *Nature.* 584:463–469. https://doi.org/10.1038/s41586-020-2588-y

Meager, A., K. Visvalingam, P. Peterson, K. Möll, A. Murumägi, K. Krohn, P. Eskelin, J. Perheentupa, E. Husebye, Y. Kadota, and N. Willcox. 2006. Anti-interferon autoantibodies in autoimmune polyendocrinopathy syndrome type 1. *PLoS Med.* 3:e289. https://doi.org/10.1371/journal.pmed.0030289

Mick, E., J. Kamm, A.O. Pisco, K. Ratnasiri, J.M. Babik, G. Castañeda, J.L. DeRisi, A.M. Detweiler, S.L. Hao, K.N. Kangelaris, et al. 2020. Upper airway gene expression reveals suppressed immune responses to SARS-CoV-2 compared with other respiratory viruses. *Nat. Commun.* 11:5854. https://doi.org/10.1038/s41467-020-19587-y

Mommert, M., M. Perret, M. Hockin, S. Viel, A. Belot, J.-C. Richard, M. Mezidi, J.-B. Fassier, E. Javouhey, A. Hemmert, et al. COVID-HCL Study Group. 2021. Type-I Interferon assessment in 45 minutes using the FilmArray® PCR platform in SARS-CoV-2 and other viral infections. *Eur. J. Immunol.* 51:989–994. https://doi.org/10.1002/eji.202048978

Ng, D.L., A.C. Granados, Y.A. Santos, V. Servellita, G.M. Goldgof, C. Meydan, A. Sotomayor-Gonzalez, A.G. Levine, J. Balcerek, L.M. Han, et al. 2021. A diagnostic host response biosignature for COVID-19 from RNA profiling of nasal swabs and blood. *Sci. Adv.* 7:eabe5984. https://doi.org/10.1126/sciadv.abe5984

Park, A., and A. Iwasaki. 2020. Type I and Type III Interferons - Induction, Signaling, Evasion, and Application to Combat COVID-19. *Cell Host Microbe.* 27:870–878. https://doi.org/10.1016/j.chom.2020.05.008

Pescarmona, R., A. Belot, M. Villard, L. Besson, J. Lopez, I. Mosnier, A.-L. Mathieu, C. Lombard, L. Garnier, C. Frachette, et al. 2019. Comparison of RT-qPCR and Nanostring in the measurement of blood interferon response for the diagnosis of type I interferonopathies. *Cytokine.* 113: 446–452. https://doi.org/10.1016/j.cyto.2018.10.023

Pierce, C.A., S. Sy, B. Galen, D.Y. Goldstein, E. Orner, M.J. Keller, K.C. Herold, and B.C. Herold. 2021. Natural mucosal barriers and COVID-19 in children. *JCI Insight.* 6:e148694. https://doi.org/10.1172/jci.insight.148694

Pizzorno, A., B. Padey, T. Julien, S. Trouillet-Assant, A. Traversier, E. Errazuriz-Cerda, J. Fouret, J. Dubois, A. Gaymard, F.-X. Lescure, et al. 2020. Characterization and Treatment of SARS-CoV-2 in Nasal and Bronchial Human Airway Epithelia. *Cell Rep Med.* 1:100059. https://doi.org/10.1016/j.xcrm.2020.100059

Platanitis, E., D. Demiroz, A. Schneller, K. Fischer, C. Capelle, M. Hartl, T. Gossenreiter, M. Müller, M. Novatchkova, and T. Decker. 2019. A molecular switch from STAT2-IRF9 to ISGF3 underlies interferon-induced gene transcription. *Nat. Commun.* 10:2921. https://doi.org/10.1038/s41467-019-10970-y

Premkumar, L., B. Segovia-Chumbez, R. Jadi, D.R. Martinez, R. Raut, A. Markmann, C. Cornaby, L. Bartelt, S. Weiss, Y. Park, et al. 2020. The receptor binding domain of the viral spike protein is an immunodominant and highly specific target of antibodies in SARS-CoV-2 patients. *Sci. Immunol.* 5:eabc8413. https://doi.org/10.1126/sciimmunol.abc8413

Robinot, R., M. Hubert, G.D. de Melo, F. Lazarini, T. Bruel, N. Smith, S. Levallois, F. Larrous, J. Fernandes, S. Gellenoncourt, et al. 2021. SARS-CoV-2 infection induces the dedifferentiation of multiciliated cells and impairs mucociliary clearance. *Nat. Commun.* 12. https://doi.org/10.1038/s41467-021-24521-x

Rosain, J., X.-F. Kong, R. Martinez-Barricarte, C. Oleaga-Quintas, N. Ramirez-Alejo, J. Markle, S. Okada, S. Boisson-Dupuis, J.-L. Casanova, and J. Bustamante. 2019. Mendelian susceptibility to mycobacterial disease: 2014-2018 update. *Immunol. Cell Biol.* 97:360–367. https://doi.org/10.1111/imcb.12210

Rydyznski Moderbacher, C., S.I. Ramirez, J.M. Dan, A. Grifoni, K.M. Hastie, D. Weiskopf, S. Belanger, R.K. Abbott, C. Kim, J. Choi, et al. 2020. Antigen-Specific Adaptive Immunity to SARS-CoV-2 in Acute COVID-19 and Associations with Age and Disease Severity. *Cell.* 183:996–1012.e19. https://doi.org/10.1016/j.cell.2020.09.038

Sallard, E., F.-X. Lescure, Y. Yazdanpanah, F. Mentre, and N. Peiffer-Smadja. 2020. Type 1 interferons as a potential treatment against COVID-19. *Antiviral Res.* 178:104791. https://doi.org/10.1016/j.antiviral.2020.104791

Schneider, W.M., M.D. Chevillotte, and C.M. Rice. 2014. Interferon-stimulated genes: a complex web of host defenses. *Annu. Rev. Immunol.* 32:513–545. https://doi.org/10.1146/annurev-immunol-032713-120231

Schultze, J.L., and A.C. Aschenbrenner. 2021. COVID-19 and the human innate immune system. *Cell.* 184:1671–1692. https://doi.org/10.1016/j.cell.2021.02.029

Stertz, S., and B.G. Hale. 2021. Interferon system deficiencies exacerbating severe pandemic virus infections. *Trends Microbiol.*:S0966-842X(21)00060-3. https://doi.org/10.1016/j.tim.2021.03.001

Szabo, P.A., P. Dogra, J.I. Gray, S.B. Wells, T.J. Connors, S.P. Weisberg, I. Krupska, R. Matsumoto, M.M.L. Poon, E. Idzikowski, et al. 2021. Longitudinal profiling of respiratory and systemic immune responses reveals myeloid cell-driven lung inflammation in severe COVID-19. *Immunity.* 54:797–814.e6. https://doi.org/10.1016/j.immuni.2021.03.005

Tawfik, D.M., L. Vachot, A. Bocquet, F. Venet, T. Rimmelé, G. Monneret, S. Blein, J.L. Montgomery, A.C. Hemmert, A. Pachot, et al. 2020. Immune Profiling Panel: A Proof-of-Concept Study of a New Multiplex Molecular Tool to Assess the Immune Status of Critically Ill Patients. *J. Infect. Dis.* 222(Suppl 2):S84–S95. https://doi.org/10.1093/infdis/jiaa248

Trouillet-Assant, S., C. Albert Vega, A. Bal, J.A. Nazare, P. Fascia, A. Paul, A. Massardier-Pilonchery, C. D Aubarede, N. Guibert, V. Pitiot, et al. COVID-SER study group. 2020a. Assessment of serological techniques for screening patients for COVID-19 (COVID-SER): a prospective, multicentric study. *BMJ Open.* 10:e041268. https://doi.org/10.1136/bmjopen-2020-041268

Trouillet-Assant, S., S. Viel, A. Gaymard, S. Pons, J.-C. Richard, M. Perret, M. Villard, K. Brengel-Pesce, B. Lina, M. Mezidi, et al. COVID HCL Study group. 2020b. Type I IFN immunoprofiling in COVID-19 patients. *J. Allergy Clin. Immunol.* 146:206–208.e2. https://doi.org/10.1016/j.jaci.2020.04.029

Troya, J., P. Bastard, L. Planas-Serra, P. Ryan, M. Ruiz, M. de Carranza, J. Torres, A. Martínez, L. Abel, J.-L. Casanova, and A. Pujol. 2021. Neutralizing

Autoantibodies to Type I IFNs in >10% of Patients with Severe COVID-19 Pneumonia Hospitalized in Madrid, Spain. *J. Clin. Immunol.* 41:914–922. https://doi.org/10.1007/s10875-021-01036-0

van der Wijst, M.G.P., S.E. Vazquez, G.C. Hartoularos, P. Bastard, T. Grant, R. Bueno, D.S. Lee, J.R. Greenland, Y. Sun, R. Perez, et al. 2021. Longitudinal single-cell epitope and RNA-sequencing reveals the immunological impact of type 1 interferon autoantibodies in critical COVID-19. *bioRxiv*. (Preprint posted March 10, 2021) https://doi.org/10.1101/2021.03.09.434529

Vanderheiden, A., P. Ralfs, T. Chirkova, A.A. Upadhyay, M.G. Zimmerman, S. Bedoya, H. Aoued, G.M. Tharp, K.L. Pellegrini, C. Manfredi, et al. 2020. Type I and Type III Interferons Restrict SARS-CoV-2 Infection of Human Airway Epithelial Cultures. *J. Virol.* 94:e00985–e20. https://doi.org/10.1128/JVI.00985-20

Wang, K., X. Zhang, J. Sun, J. Ye, F. Wang, J. Hua, H. Zhang, T. Shi, Q. Li, and X. Wu. 2020. Differences of Severe Acute Respiratory Syndrome Coronavirus 2 Shedding Duration in Sputum and Nasopharyngeal Swab Specimens Among Adult Inpatients With Coronavirus Disease 2019. *Chest.* 158:1876–1884. https://doi.org/10.1016/j.chest.2020.06.015

Wilson, D.H., D.M. Rissin, C.W. Kan, D.R. Fournier, T. Piech, T.G. Campbell, R.E. Meyer, M.W. Fishburn, C. Cabrera, P.P. Patel, et al. 2016. The Simoa HD-1 Analyzer: A Novel Fully Automated Digital Immunoassay Analyzer with Single-Molecule Sensitivity and Multiplexing. *J. Lab. Autom.* 21:533–547. https://doi.org/10.1177/2211068215589580

Zhang, Q., P. Bastard, A. Bolze, E. Jouanguy, S.-Y. Zhang, A. Cobat, L.D. Notarangelo, H.C. Su, L. Abel, and J.-L. Casanova. COVID Human Genetic Effort. 2020a. Life-Threatening COVID-19: Defective Interferons Unleash Excessive Inflammation. *Med (N Y).* 1:14–20. https://doi.org/10.1016/j.medj.2020.12.001

Zhang, Q., P. Bastard, Z. Liu, J. Le Pen, M. Moncada-Velez, J. Chen, M. Ogishi, I.K.D. Sabli, S. Hodeib, C. Korol, et al. NIAID-USUHS/TAGC COVID Immunity Group. 2020b. Inborn errors of type I IFN immunity in patients with life-threatening COVID-19. *Science.* 370:eabd4570. https://doi.org/10.1126/science.abd4570

Ziegler, C.G.K., V.N. Miao, A.H. Owings, A.W. Navia, Y. Tang, J.D. Bromley, P. Lotfy, M. Sloan, H. Laird, H.B. Williams, et al. 2021. Impaired local intrinsic immunity to SARS-CoV-2 infection in severe COVID-19. *Cell.* https://doi.org/10.1016/j.cell.2021.07.023

Supplemental material

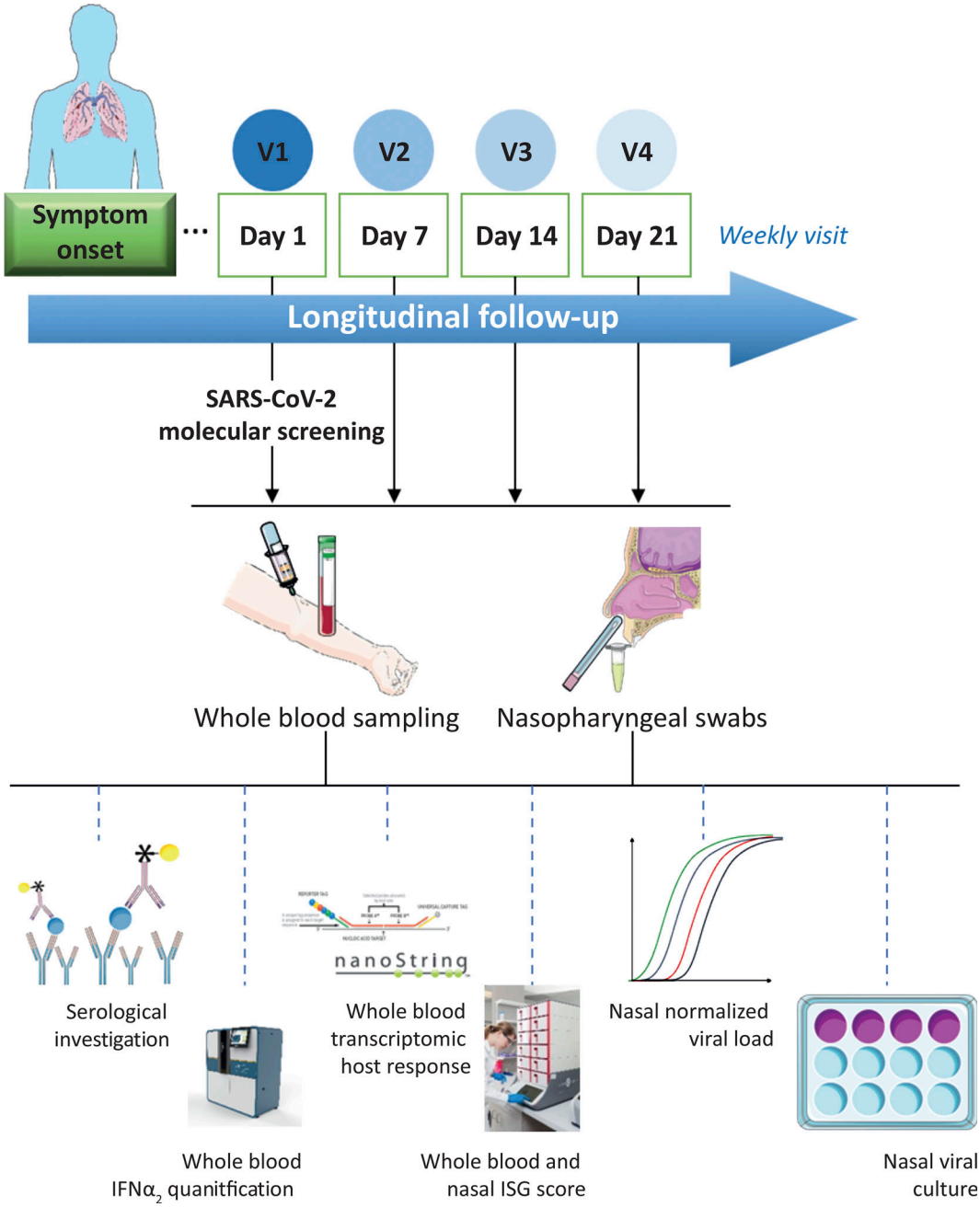

Figure S1. **Graphical outline of the study.** Parts of the figure were drawn by using pictures from Servier Medical Art (http://smart.servier.com/), licensed under a Creative Commons Attribution 3.0 Unported License (https://creativecommons.org/licenses/by/3.0/). Simoa HD-1 illustration used with permission from Quanterix and Nanostring.

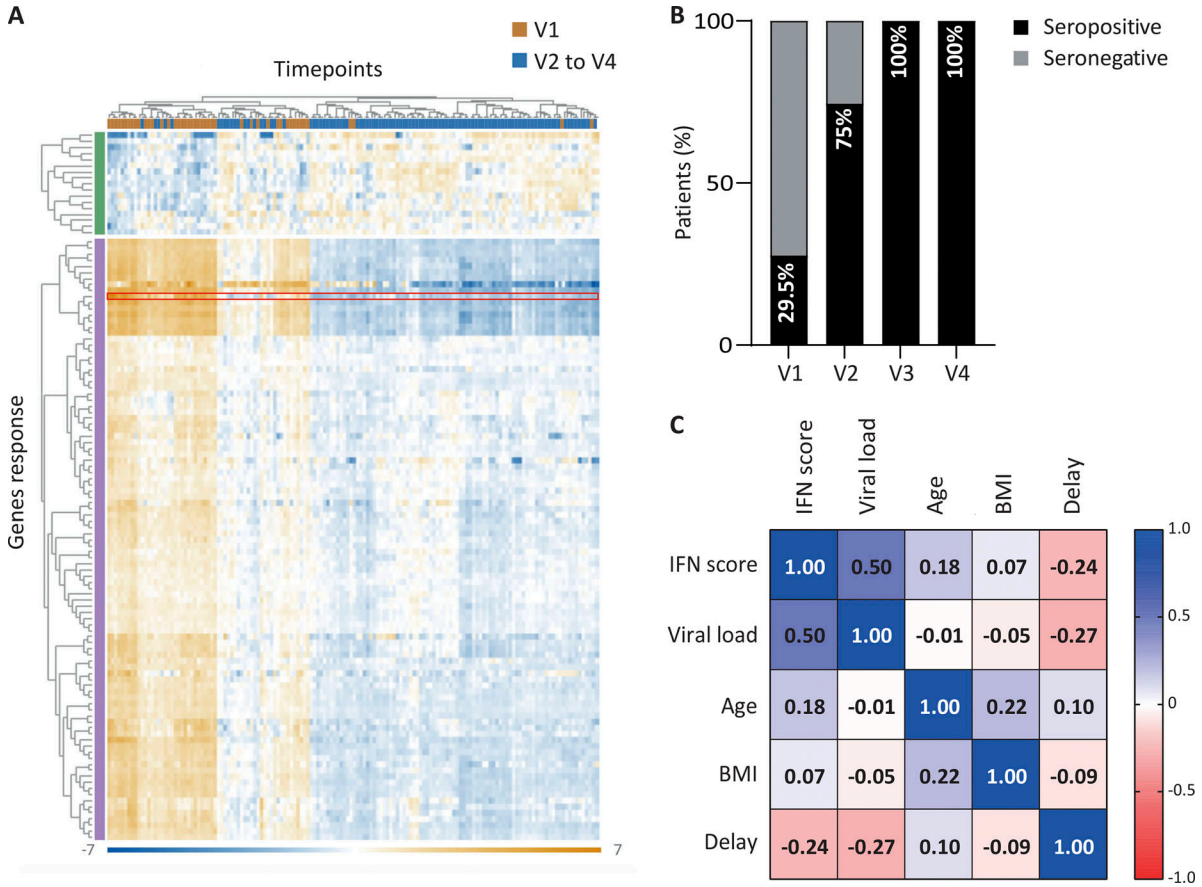

Figure S2. **Whole-blood transcriptomic analysis at different time points post-diagnosis. (A)** Unsupervised clustering of V1 (orange columns) and V2–V4 samples (blue columns) and DEGs, measured using the NanoString host response panel. The green vertical bar highlights the 17 genes down-regulated at V1 compared with V2/V3/V4, and the purple bar highlights the 106 genes up-regulated at V1 compared with V2/V3/V4. **(B)** Histogram bars showing the percentage of seroconverted (Wantai total SARS-CoV-2 Ig) patients within the cohort of mildly symptomatic COVID-19 health care workers at the different time points of the longitudinal follow-up. **(C)** Pearson correlation table between NanoString IFN score, nasal viral load, age, body mass index (BMI), and delay after symptoms.

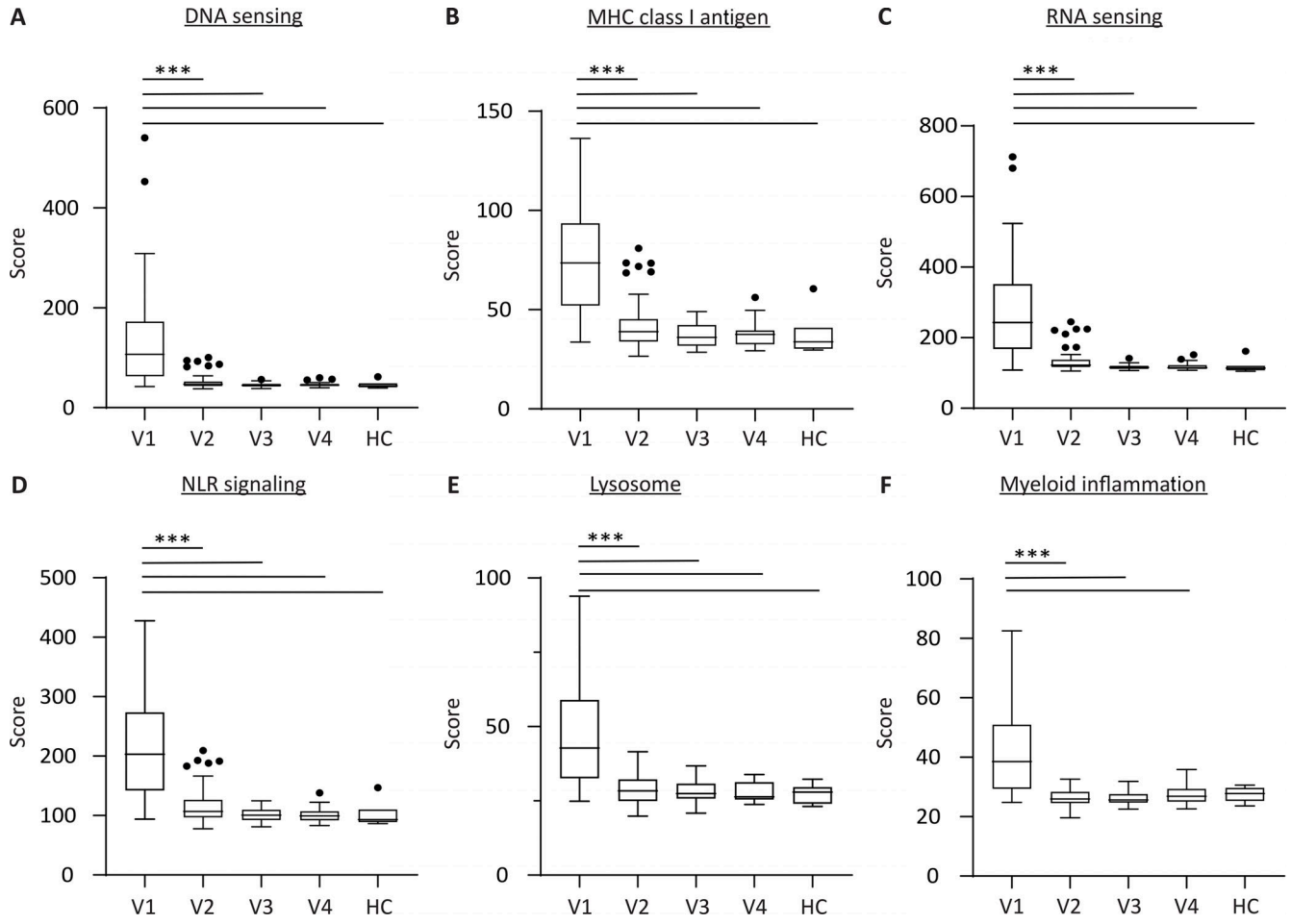

Figure S3. **Dynamics of induction in the blood of different immune pathways during SARS-CoV-2 infection. (A–F)** Boxplots showing the blood expression score for different pathways significantly modulated from V1 to V4. A Kruskal–Wallis with uncorrected Dunn's test was used for statistical analysis of data presented in this figure (multiple comparisons; ***, P < 0.001).

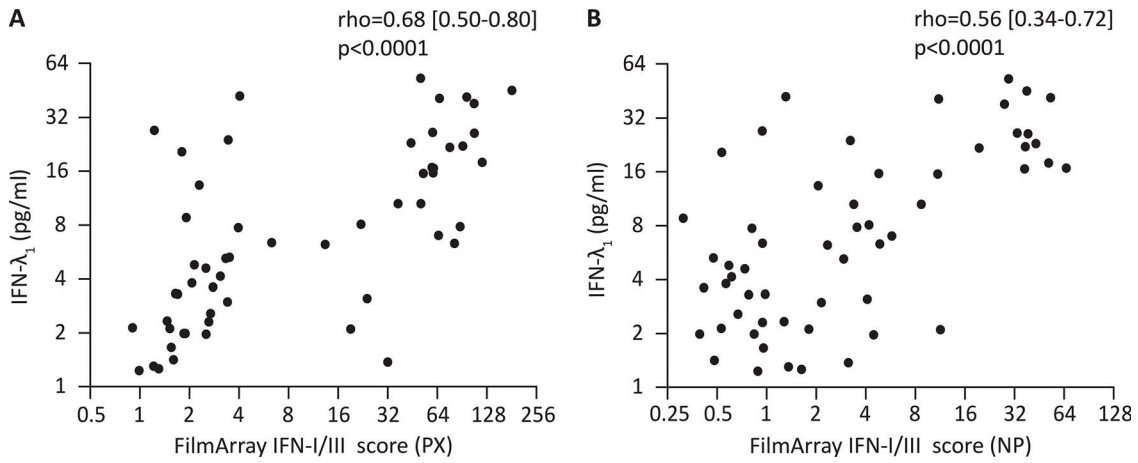

Figure S4. **Correlation between IFN-I/III scores and serum I IFN-λ_1 levels. (A and B)** Correlation between the blood (A; PX) or NP (B) IFN-I/III scores and plasmatic IFN-λ_1 levels (n = 56 samples with a detectable value from 22 patients), determined by ELISA. The Spearman's correlation coefficient is shown.

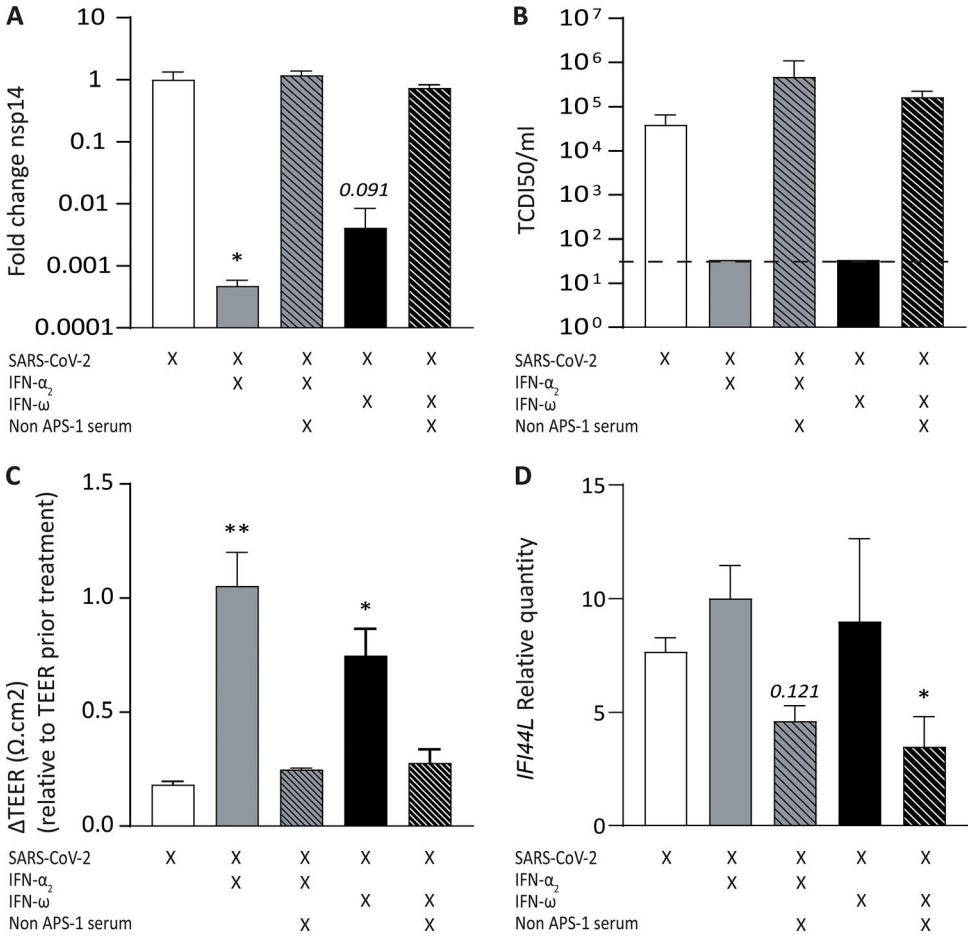

Figure S5. **Sera containing anti–IFN-I antibodies neutralize IFN-α_2 antiviral activity in a reconstituted HAE model of SARS-CoV-2 infection.** The effect of a serum from a non–APS-1 patient containing IFN-I auto-Abs was evaluated in a reconstituted HAE model of SARS-CoV-2 infection. **(A)** Nasal HAEs were treated (24 h before and 1 h after SARS-CoV-2 infection) with recombinant IFN-α_2 in the presence or absence of the indicated sera. Apical washes were performed 54 hpi, and viral titers were determined by RT-PCR. Results are representative of three biological replicates and expressed as relative to the mock-treated control. **(B)** Apical infectious viral titers 54 hpi determined by TCID50. The dotted line depicts the limit of detection. **(C)** Δ TEER between t = 0 and t = 54 hpi. **(D)** Relative expression of *IFI44L* assessed using FilmArray technology from total cellular RNA extracted after infection. In the figure, bars and error bars represent mean and SD, respectively. A Kruskal–Wallis with uncorrected Dunn's test was used for statistical analysis of data presented in this figure (multiple comparisons; *, P < 0.05; **, P < 0.01). In all conditions, the reference condition was SARS-CoV-2 alone (white bars).

Tables S1 and S2 are provided online as separate Excel files, and Table S3 is provided online as a separate PDF. Table S1 lists all genes whose expression is measured in the host response NanoString panel and functional annotation of these genes. Table S2 lists genes differentially expressed between blood cells in mild COVID-19 patients at diagnosis and blood cells from HCs. Table S3 is a 2 × 2 contingency table relative to IFN-α auto-Ab detection from nasal and plasma paired samples from mildly symptomatic and critically ill COVID-19 patients.